Direct Utilization of Coal Syngas in High Temperature Fuel Cells

DOE EPSCoR - WV State Implementation Program

Final Report

October 2014

Project Director / Administrative PI: Richard A. Bajura (NRCCE, WVU)

Technical PI: Ismail Celik (MAE, WVU)

DOE Program Manager: Tim Fitzsimmons (BES, DOE)

Collaborating DOE Office: Briggs White (NETL, DOE)

Contact Information

Dr. Ismail Celik West Virginia University Department of Mechanical & Aerospace Engineering Phone: (304) 293-3209 Ismail.celik@mail.wvu.edu

Foreword

This research program was supported in two phases. During Phase I (FY 2006 – FY 2009), we established our laboratory facilities, initiated model development, and identified the major constituents that affect fuel cell performance. These results were reported previously. The Phase II program (FY 2009 – FY 2014) is summarized in the present report.

The research team members contributing to this final report consists of the persons identified in the table below.

Investigator	Affiliation*	Research Area			
		Characterization of contaminant effects	Continuum Modeling	Anode Material Development	Management
PIs					
Richard A. Bajura	NRCCE				✓
I. Celik	MAE		✓		✓
B. Kang	MAE	✓	✓		✓
X. Liu	MAE	✓		✓	
N. Wu	MAE	✓			
E. Sabolsky	MAE	✓		✓	
J. Zondlo	CHE	✓		✓	
H. Finklea	Chem	✓			
X. Song	MAE	✓			
Post Doctoral Fellows					
S. Raju Pakalapati	MAE		✓		
Graduate Research Students					
Hayri Sezer	MAE		✓		

*The acronyms used to define the affiliation of the team members is described below:

CHE: Department of Chemical Engineering of Benjamin M. Statler College of Engineering and Mineral Resources
Chem: Department of Chemistry of Eberly College of Arts and Sciences
MAE: Department of Mechanical and Aerospace Engineering of Benjamin M. Statler College of Engineering and Mineral Resources
NRCCE: National Research Center for Coal and Energy at WVU

Summary

This EPSCoR project had two primary goals: (i) to build infrastructure and work force at WVU to support long-term research in the area of fuel cells and related sciences; (ii) study effects of various impurities found in coal-syngas on performance of Solid Oxide Fuel Cells (SOFC). As detailed in this report the WVU research team has made significant accomplishments in both of these areas. What follows is a brief summary of these accomplishments:

State-of-the-art test facilities and diagnostic tools have been built and put into use. These include cell manufacturing, half-cell and full-cell test benches, XPS, XRD, TEM, Raman, EDAX, SEM, EIS, and ESEM equipment, unique in-situ measurement techniques and test benches (Environmental EM, Transient Mass-Spectrometer-MS, and IR Optical Temperature measurements). In addition, computational capabilities have been developed culminating in a multi-scale multi-physics fuel cell simulation code, DREAM-SOFC, as well as a Beowulf cluster with 64 CPU units.

We have trained 16 graduate students, 10 postdoctoral fellows, and recruited 4 new young faculty members who have actively participated in the EPSCoR project. All four of these faculty members have already been promoted to the tenured associate professor level. With the help of these faculty and students, we were able to secure 14 research awards/contracts amounting to a total of circa $5.0 Million external funding in closely related areas of research.

Using the facilities mentioned above, the effects of PH_3, HCl, Cl_2, and H_2S on cell performance have been studied in detail, mechanisms have been identified, and also remedies have been proposed and demonstrated in the laboratory. For example, it has been determined that PH_3 reacts rapidly with Ni to from secondary compounds which may become softer or even melt at high temperature and then induce Ni migration to the surface of the cell changing the material and micro-structural properties of the cell drastically. It is found that the extent of steam and current load accelerate the degradation caused by PH_3. A unique filtering technique has been proposed to reduce the effect of PH_3. In addition, various cell materials have been proposed to reduce the rate of degradation caused by H_2S.

Furthermore, a three-dimensional, transient multi-physics model has been formulated to describe primary transport processes and electro-chemical reactions occurring within the cell. This model has been validated using data gathered from accelerated tests. The validated model then has been used to study the degradation rates under a range of operating conditions and impurity levels. This has resulted in a procedure that uses both experiments and simulations to predict the life-time of a cell operating with syngas with known concentration of trace impurities.

Finally all the experience and knowledge gained has been disseminated via 39 journal papers and 43 presentations/posters/conference papers.

Table of Contents

1. Introduction

It has been established that the process of degradation is a strongly non-linear phenomenon, especially when multiple contaminants are active simultaneously [1], [2], [3]. The challenging question of 'what is the maximum contaminant concentration that can be tolerated by a given fuel cell with a reasonably long duration of operation?' still remains unanswered. Even though it is possible to produce ultra-clean syngas by application of modern gas-clean-up technology, the cost of reducing all potentially harmful contaminants to sub-ppm levels will be very high. It is then essential to establish maximum tolerance levels for commonly used SOFCs running safely on various compositions of coal syngas under a range of operating conditions without shutdown and unreasonable maintenance costs. Given the fact that there are tens of trace species present in coal syngas, it seems practically impossible to establish such a matrix only by testing since the degradation process is very slow at low concentrations, and each case may need testing times in the order of thousands of hours. The best possible route of research to move forward is to optimize the knowledge base gained from short-term testing at relatively higher concentrations, and use this knowledge base to develop models that can be used to predict degradation levels at any composition at any time. The models must be based on experimental data and on the chemical and physical processes occurring mainly in the active layer of the anode. At the same time, the tolerance levels to contaminant exposure can be increased by exploring novel anode materials. Based on these observations the following objectives were set for the WV EPSCoR project.

Predict the life time of the Ni/YSZ anode operated in impurity-containing syngas

(1.1) What is the tolerant limit of the Ni/YSZ anode for a specific impurity?

(1.2) What is the life time of the Ni/YSZ anode if the concentration of a specific impurity exceeds the tolerant limit?

In addition to satisfying the above objectives, the team also extended the work to include:

Development of additional in-situ and ex-situ methods for characterization of gas composition and cell chemistry/structure

Development of methods for remediation or mitigation of the impurity poisoning effect

Extension of the study to explore the possibility of using biogas as a fuel in SOFCs

The long term goal is to enable the use of coal-derived syngas as a source of clean and environmentally friendly energy generation.

Our research effort focused on three primary areas of investigation: characterizing the effects of contaminants on fuel cell performance; constructing continuum models to describe the performance of the fuel cell from micro scale to large scale planar units; and, developing usable anode materials. The following seven sections describe the work we have accomplished over the five years of Phase II. Appendix A is a supplementary report that describes the accomplishments of our last year's effort, which has not been reported in detail previously.

Appendix B contains a list of graduate students and postdoctoral fellows who contributed to the Phase II effort, as well as other summary information such as publications, patents, and follow-on supported research projects.

2. Accelerated Testing/Techniques for Performance Degradation

In this section are described studies of nanoscale structural studies in the presence and absence of syngas, in-situ measurements of strain and temperature on an operating SOFC in clean hydrogen and syngas, further degradation studies based on the electrochemical performance of the SOFC, and mass spectroscopic analyses of the fuel gases with and without PH_3 as a function of temperature and humidity.

2.1. Microstructural and chemical evolution of anode grain boundaries and triple phase boundary (TPB) junctions of Ni/YSZ anode supported solid oxide fuel cells.

Systematic microstructure and chemical analyses were conducted of the anode, from microns to the atomic scale, before and after exposure to syngas with combinations of contaminants at different operating conditions. The microstructural analysis was performed using advanced analytical electron microscopy including Transmission Electron Microscopy (TEM) equipped with Energy Dispersive X-ray Spectroscopy. This comprehensive microscopic and spectroscopic characterization provided a better understanding of the chemical and physical processes involved in the SOFCs operation, which, in turn, facilitated accurate physics-based modeling in addition to optimization of SOFC performance.

A NiO phase was found to develop along the Ni/YSZ interfaces extending to TPBs in the operated cells at 800°C. The thickness of the NiO ribbon phase remains constant at ~5 nm in hydrogen for operating durations up to 540 h. When operating on synthesis gas, an increase in interphase thickness was observed from ~11 nm for 24 h of operation to ~51 nm for 550 h of operation, as shown in Figure 2.1.

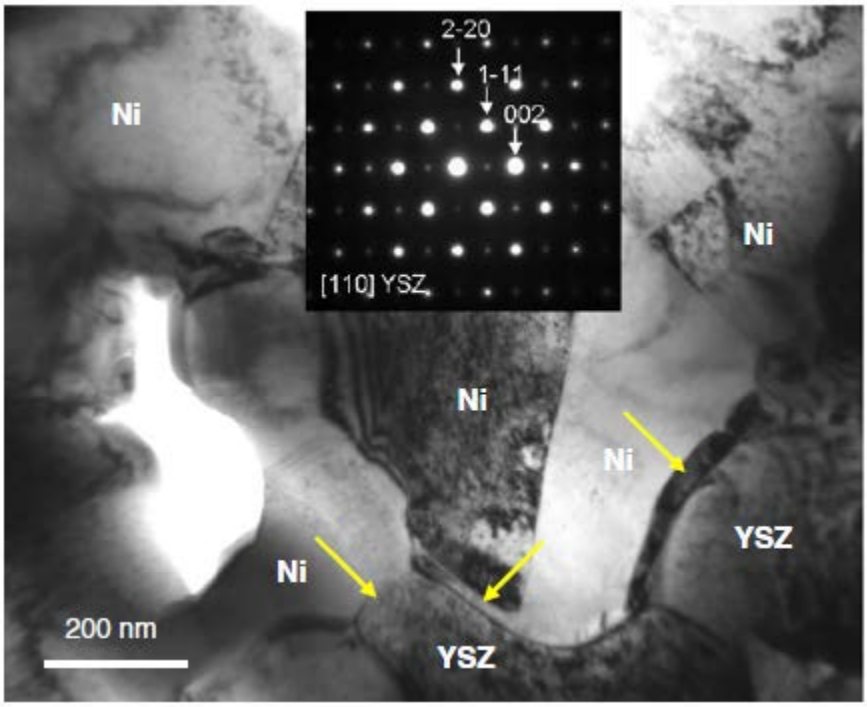

Figure 2.1: Electron diffraction pattern and the diffraction contrast image taken from the anode of 550 h operated cell at 800°C. An inter-granular ribbon phase between YSZ and Ni can be observed and is pointed out by yellow arrows.

YSZ phases are observed to be stable in H_2 over 540 h of operation. However, for the cell operated in syngas for 550 h, a 5–10 nm tetragonal YSZ (t-YSZ) interfacial layer was identified that originated from the Ni/YSZ interfaces. Yttrium species seem to segregate to the interfaces during operation, leading to the formation of t-YSZ in the Y-depleted regions.

2.2. Microstructural and crystallographic defects of YSZ in the anode (Ni/YSZ)

Solid oxide fuel cell (SOFC) electrolytes must be crystallographically and chemically stable in typical operating environments, while also possessing high ionic and low electronic conductivities. Cubic fluorite structured yttria-stabilized zirconia (YSZ), in which ion conduction is provided by oxide ion vacancies, is a proven oxide ion conductor fulfilling such requirements. The microstructural and crystallographic defects of YSZ in the anode (Ni/YSZ), cathode (LSM/YSZ), and electrolyte of commercial SOFC cells were studied using TEM.

Examination of the measured YSZ electron diffraction pattern of the cathode revealed a typical cubic fluorite crystal structure. However, weak diffraction spots, where diffractions should be absent according to the structure factor of the cubic fluorite phase, are present in the patterns taken from the YSZ in the anode and the electrolyte. The appearance of kinematically forbidden spots in YSZ is unchanged after cell operation. Such weak diffraction spots can be interpreted as arising from nanoscale (2–10 nm) irregularly-shaped tetragonal YSZ (t-YSZ) domains that are randomly distributed in the cubic YSZ (c-YSZ) matrix, as shown in Figure 2.2.

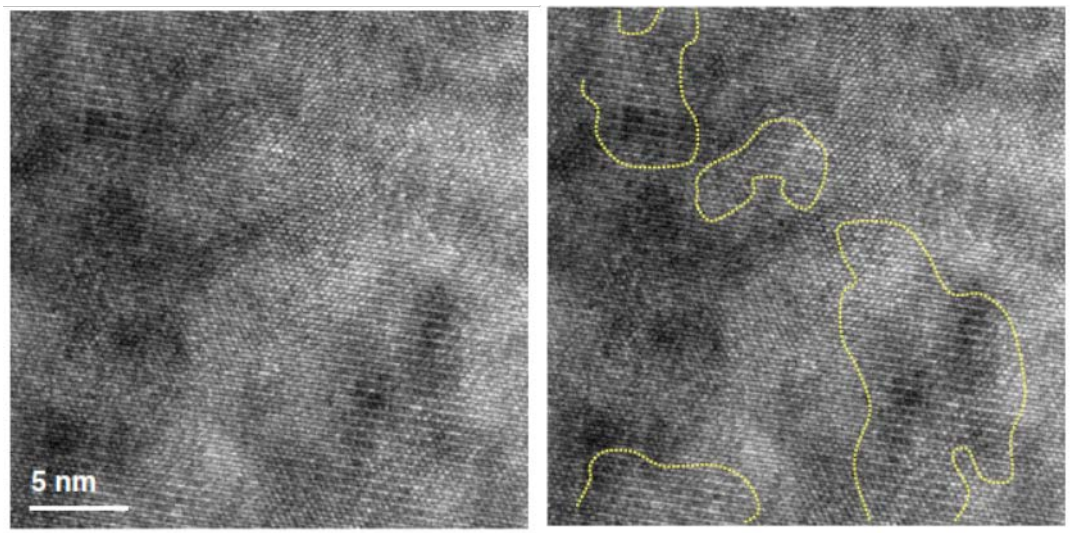

Figure 2.2: High resolution TEM image taken from the YSZ in the anode side, and same HRTEM image with dot lines circling the regions where clearly feature t-YSZ domains.

2.3. Full Cell Tests

An optical setup, based on the phase-shift Sagnac Interferometry method, has been developed and applied to obtain out-of-plane deformation of button cells exposed to coal syngas with and without impurities whereby EIS, ASR and IR measurements can be performed simultaneously. Figure 2.3 shows interferometric fringe patterns on Ni wire mesh located at 5.5mm away from the center of the button cell with different applied pressures at room temperature (RT) and high temperature (800 ^{o}C) respectively. From these measured fringe patterns, the change in slope per unit applied pressure ($\Delta S/\Delta P$) is 3.82×10^{-5} per psi at RT was calculated. The results showed good agreement with the FEA numerical and analytical results (Figure 2.4), with an error of less than 5%. Similar results are obtained for high temperature measurement at 800 ^{o}C ($\Delta S/\Delta P = 5.95\times 10^{-5}$). The results from these observations are used to validate the SOFC structural and electrochemical models developed under Project 2.

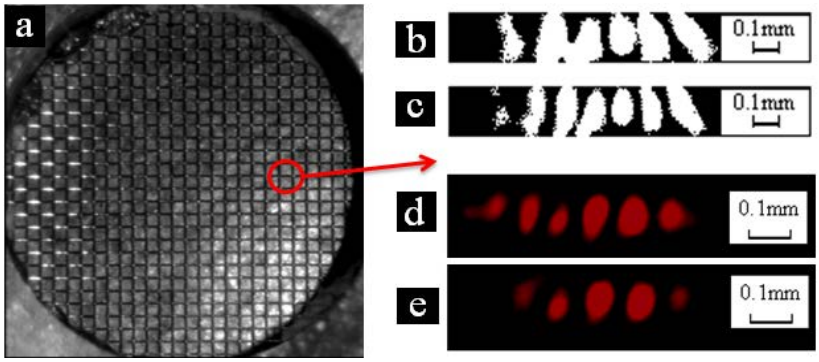

Figure 2. 3: (a) Ni mesh image on a SOFC button cell and Fringe patterns on Ni mesh at r = 5.5 mm from the center using NexTech Probostat™ test apparatus with different applied pressures: (b) 0 psi and (c) 19 psi at RT, (d) 5 psi and (e) 15 psi at 800 ^{o}C

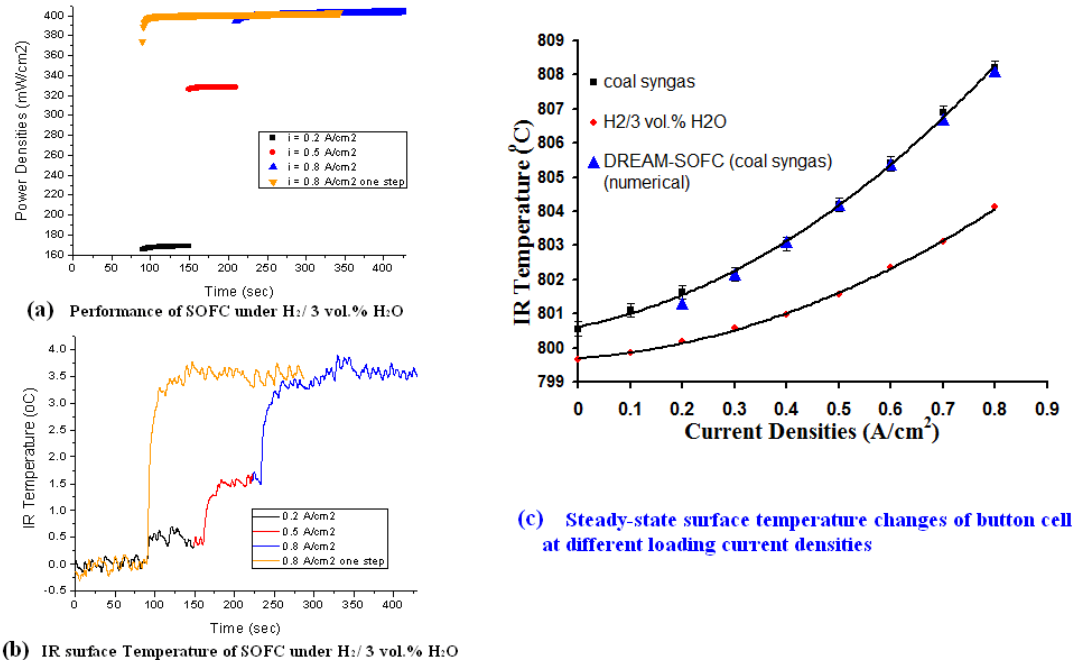

Figure 2.4: (a) Power densities history of button cell (b) Corresponding transient temperature changes under different loading current densities interval under 100 sccm H_2/3 vol.% H_2O; and (c) Steady-state surface temperature changes of button cell at different loading current densities with different fuel gases

Button cell surface temperatures were monitored as a function of applied current densities in hydrogen and simulated clean coal syngas. Figure 2.4 shows the surface temperature change of a button cell under 100 sccm H_2/3 vol.% H_2O. The cell surface temperature increases with increase in current density and it takes about 20 to 60 seconds to reach steady state temperature depending on the applied current density. As shown in Figure 2.4(a & b), the final steady state surface temperature is independent of the intermediate current steps and only depends on the final current density (0.8 A/cm^2) but takes less time to reach the steady state temperature when current is applied in large steps. The change of the steady-state cell surface temperature is plotted against loading current densities in Figure 2.4(c), and shows that the cell temperature increases non-linearly with the current density. Similar results are obtained under 100 sccm clean coal syngas. These experimental results are useful for validation of button cell electrochemical reaction simulations. The simulations indicate that the major source of the temperature rise is entropic heating from fuel oxidation and a minor source is ohmic heating, while the water gas shift reaction provides a negligible contribution in a syngas condition.

Comparison tests were conducted in which button cells were exposed to ppm level of PH_3 under dry and wet hydrogen conditions with loading potential bias. Electrochemical and microstructural analyses were performed to study long-term PH_3 poisoning effect on SOFC performance at 800^{o}C. Figure 2.5 (a) shows the variation of SOFC power density history at constant loading current density of 0.7 A/cm^2 over time. In this experiment, the cell was initially exposed to dry hydrogen gas and then 10 ppm of PH_3 was injected into the fuel gas for 48 hrs. It can be seen that the cell power density remained almost constant during exposure to PH_3 with dry H_2. The cell performance showed faster degradation when steam was introduced into the fuel gas. The power density of button cell decreased gradually over time, e.g. 0.12 mW/cm^2 per hour degradation under H_2/3 vol.% H_2O with 10 ppm PH_3. It also illustrated that the cell performance degradation was more severe under higher steam content in the PH_3-containing fuel gas.

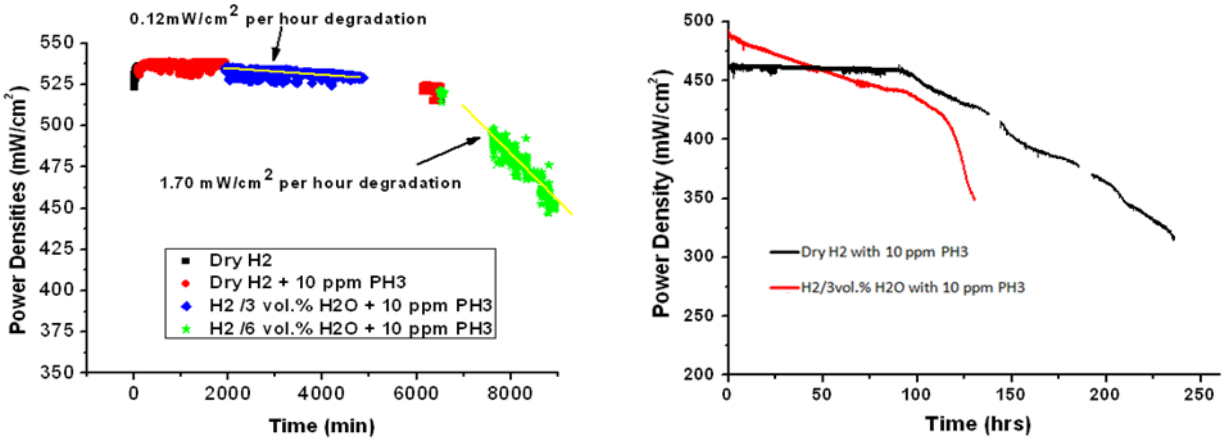

(a) (b)

Figure 2.5: Variation of SOFC power density under different testing conditions

Longer PH_3 exposure tests are illustrated in Figure 2.5 (b). The black curve shows the long term PH_3 effect with dry hydrogen at 0.6 A/cm^2 applied current density. The cell performance remained stable for the first 4 days under exposure of dry hydrogen/PH_3. For the next 6 days, the cell performance degraded at a rate of 0.43 mW/cm^2 per hour. The dominant performance degradation was in the polarization resistance which increased by 267% in 240 hrs. The cell failed sharply within one day due to cracking. Similar to the results shown in Figure 2.5 (a), it can be seen from the red curve shown in Figure 2.5 (b) that the cell performance degrades immediately once the steam is added into the fuel gas. The cell performance degraded at a faster rate (0.54 mW/cm^2 per hour) as compared to 0.43 mW/cm^2 per hour in dry hydrogen with same PH_3 level. The degradation rate was affected by increases in the polarization resistance (180%) and the ohmic resistance (119%) over 150 hours. It can be concluded that humidity and phosphine operate synergistically to accelerate SOFC degradation.

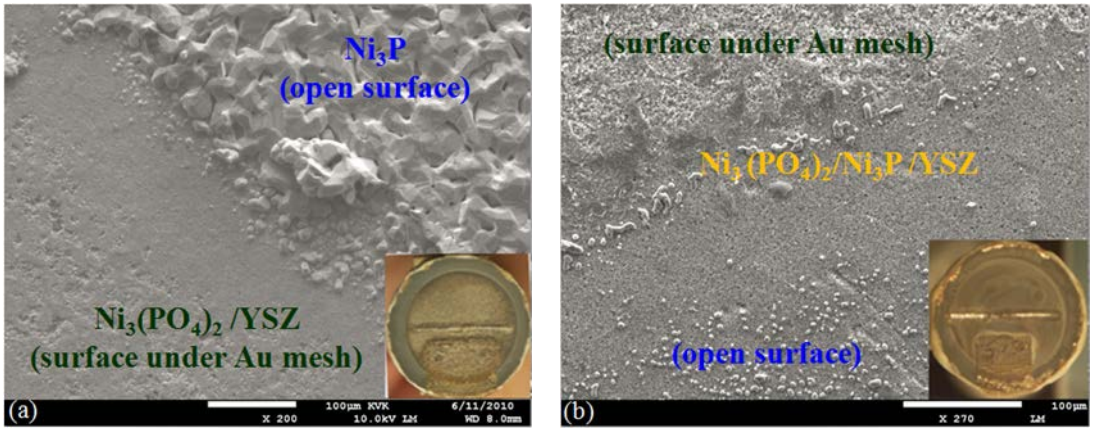

Figure 2.6: SEM Micrograph of the anode surface after exposure to 10 ppm PH_3 at i = 0.6 A/cm^2 in (a) H_2/3 vol.% H_2O for 9 days and (b) dry H_2 for 11 days

The secondary phase formation and microstructure reconstructions were confirmed via the post-term characterization (i.e. SEM, XRD), as shown in Figure 2.6. Both nickel phosphide and nickel phosphate were present. The presence of current collector appeared to affect which phase was formed. The loss of nickel from the anode, the presence of a dense nickel compound on the anode surface, and possibly the blocking of sites for fuel oxidation by nickel compounds can explain the fuel cell performance degradation.

2.4. In Situ Gas Concentration Measurements

Clearly as shown above, phosphine causes degradation of Ni/YSZ anodes when it is present in the fuel at ppm levels. As noted in section 2.3, the rate of degradation appears to correlate with the presence or absence of water in the fuel mixture. The new phases that appear on the anode surface can either be nickel phosphides (reduced phosphorus) or nickel phosphates (oxidized phosphorus). Consequently, there are questions on the nature of the phosphorus species reaching the anode as a function of the fuel composition. The primary objective of this sub-project is to use a mass spectrometer to determine the fate of phosphine in "dry" and "wet" fuel mixtures as a function of temperature of the gas mixture and the presence and absence of Ni/YSZ. The second objective is to monitor the fate of phosphine as it impinges on the Ni/YSZ anode in a functioning SOFC.

Experiments with the mass spectrometer interfaced with several test stands demonstrated the presence of gas leaks between the fuel and air. To avoid the leak problem, experiments were performed with alumina tubes mounted in tube furnaces with no SOFCs present, and with only fuel entering and exiting the alumina tubes. Three configurations were tested. The first configuration was a straight alumina tube with the fuel entering on one side and exiting the other side. The second configuration was the Probostat SOFC test stand without the SOFC. Fuel entered the anode entrance port and exited the cathode exhaust port. In both of these configurations, the tube furnace was programmed to heat slowly from room temperature to 800ºC, hold at this temperature for hours, and then cool back to room temperature over hours. In some experiments, a ~1 cm^2 piece of NiO/YSZ from an anode-supported half-cell was placed inside the alumina tube close to the point where a SOFC would be mounted. Linear gas flow velocities were slow enough that the gas temperature was equilibrated with the furnace temperature by the time the fuel reached the NiO/YSZ piece. In the third configuration, an electrolyte-supported SOFC was mounted in the Probostat. The mass spectrometer analyzed the anode exhaust.

All results below were acquired using the MKS Cirrus reactive gas analyzer. This system includes a meter-long heated (150ºC) capillary which permits sampling of gas mixtures at 1 atm of pressure. The unit has a mass range (m/z) of 1 to 100 with unit mass resolution. With two detectors (Faraday cup and electron multiplier), the Cirrus unit can measure partial pressures between 1 atm and 0.0001 torr. The displayed pressure in torr was routinely calibrated at mass 28 and 29 using nitrogen in air. All other masses are uncalibrated. The magnitude of the signal at a given mass was confirmed to be linear with respect to concentration of the substance with that mass. Gas sources included high purity helium, hydrogen, a blend of hydrogen with 40 ppm phosphine, and a humidifier. In "dry" hydrogen mixtures, typical impurity levels are on the order of ~1 torr for H_2O, <1 torr for N_2, and <0.5 torr for O_2. O_2 has a mass 34 isotope with a natural abundance of 0.4% which coincides with the mass 34 of PH_3. Corrections for this overlap were performed. See Figure 2.7 and Figure 2.8.

Hypotheses: PH_3 appears to react with O_2 (note how P(32) tracks P(34) in Figure 2.7), and may react with H_2O, although there are no visible correlations of P(18) with P(34). The reaction equilibrium favors products at intermediate temperatures and reactants at low and high temperatures. Also in "wet" hydrogen, the equilibrium of the reaction of PH_3 with O_2 and/or H_2O favors the products at all temperatures above 300ºC. A summary of observations are provided:

1. At room temperature, PH_3 does not react with alumina, O_2, H_2O, NiO or Ni. In all measurements below, the reaction of PH_3 is reversible with temperature, with the mass 34 signal returning to base values upon cooling to room temperature. In all measurements, the same pattern of reactivity was obtained using a quartz tube, so the tube walls are not likely controlling the reactions. In "dry" hydrogen, PH_3 appears to react between 400ºC and 600ºC, but not at higher temperatures (Figure 2.7).

2. In "wet" hydrogen, PH_3 reacts in the temperature range of 300-800ºC, with no recovery at high temperatures .
3. The presence of Ni reduces the measured amount of PH_3 at higher temperatures. The reduction of NiO to Ni is detected by a spike in H_2O signal (mass 18) in the 300-600ºC range (Figure. 2.8).
4. In particular, possible products HPO (mass 48), HPO_2 (mass 64) and HPO_3 (mass 80) are not detected. The reaction products must either be nonvolatile or have a mass above 100 (e.g., P_4O_{10}).
5. After prolonged exposure of the Probostat to PH_3 gas, clean dry hydrogen gas passing through the Probostat exhibits signals indicating the presence of PH_3 in the exhaust gas. The signals are greatly attenuated at lower temperatures, at lower partial pressures of hydrogen and in the presence of 10 torr of water. Extensive washing of the internal surfaces of the Probostat with water and acetone did not eliminate the signal. Tentatively, the signal is attributed to the reaction of hydrogen with a phosphorus solid impurity inside the Probostat.
6. The data indicate that phosphine does reach the anode of a SOFC if the fuel is "dry" (water partial pressure of 1 torr or less). However, the data do not show what species gets to the anode in "wet" fuel.
7. With an operating SOFC in the Probostat, no PH_3 or decomposition products were detected in the anode exhaust with or without 10 ppm PH_3 present at the anode inlet. Given the rapid reaction of PH_3 with nickel noted in (3) above, this observation is not surprising. Water pressures in the exhaust rise dramatically when current flow through the SOFC. No significant degradation in cell performance was observed in dry or "wet" hydrogen with added PH_3 during ~10 hours of testing.

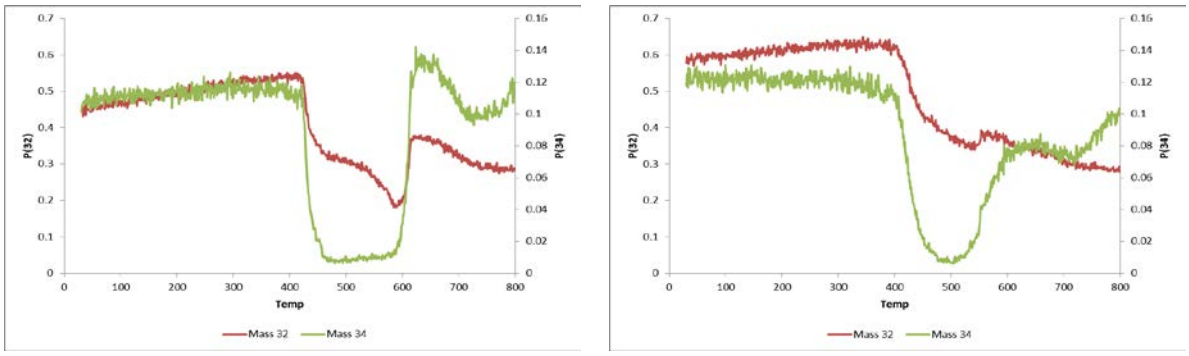

Figure 2.7 P vs T plots for an empty alumina tube during heating (left) and cooling (right) steps.

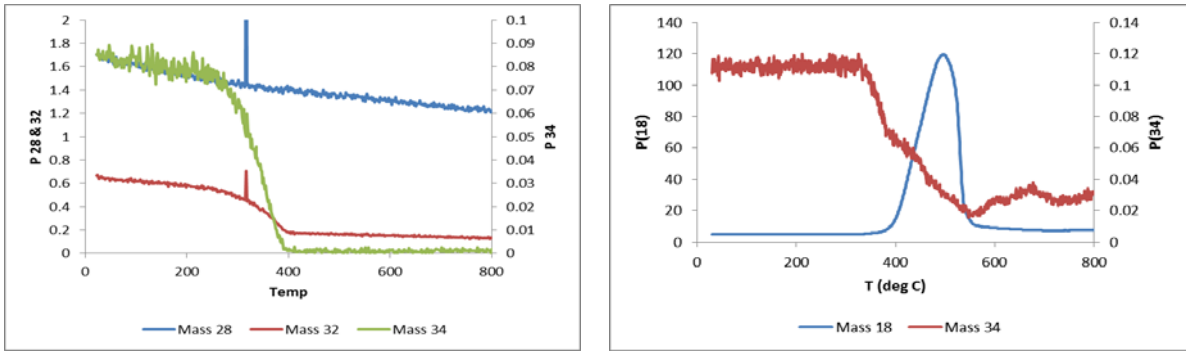

Figure 2.8: P vs temperature for an alumina tube containing a piece of NiO/YSZ anode.

3. Mechanisms for PH3 Degradation

3.1. Half Cell Tests of PH_3 degradation

This study examined the effects of the electrical current and the water content on the degradation behavior of the Ni-YSZ anode in PH_3-containing coal syngas using somewhat different methodologies then described in the previous section. The first aim was to check whether the electric current would affect the formation of the Ni-P impurity. The second aim was to examine how the water content in the coal syngas would affect the product resulting from the interaction of the Ni-YSZ anode with PH_3. When the cell was operated at a constant current loading of 0.25 A/cm^2 in the wet coal syngas containing 5 ppm PH_3, the impedance increased quickly with prolonged operation time, implying rapid degradation of the cell performance. To quantify the cell degradation based on impedance spectra at various conditions, the following equation can be used for measuring the polarization resistance change:

$$D = \frac{R_{p1} - R_{p0}}{R_{p0}} \times 100\% \quad (1)$$

where R_{p0} is the polarization resistance of the cell in the clean syngas, and R_{p1} represents the polarization resistance of cell at a given time interval. Figure 3.1 shows the polarization resistance change as a function of the operation time at different conditions. When the cell was operated in the dry coal syngas with a current loading, the degradation rate was reduced to 4.6% per hour. When the cell was operated without current loading in the wet coal syngas containing 5 ppm PH_3, the degradation rate increased to 11.9% per hour, which indicated the water content had significant effect on the degradation of the anode. The cell which was operated at a constant current loading of 0.25 A/cm^2 in the wet coal syngas containing 5 ppm PH_3, showed the largest degradation rate (24.3% per hour). The electric current clearly exacerbated the degradation of the electrochemical performance.

Figure 3.2(a) shows the SIMS images of ion fragments obtained from the cross section of Ni-YSZ anode with a current loading after operation in the wet coal syngas containing 5 ppm PH_3. Figure 3.3(a) represents the line profiles of ion fragments shown in Figure 3.2(a). It can be seen from Figure 3.2(a) and 3.3(a) that Zr^+ was depleted in the anode under the current loading after exposure to PH_3. There was almost no Zr^+ near the anode surface. Ni^+ was enriched near the anode surface. PO^- clusters were present throughout the cross-section of the Ni-YSZ anode. In addition, PO_2^- and PO_3^- clusters were observed. These results imply that zirconia was lost and nickel phosphate compounds were formed during exposure to PH_3. When the fuel cell was operated without current loading, the scenario was better, as confirmed by the line profiles of ion cluster in the cross-section of anode (Figure 3.3(b)). Ni_3P^+ was found in the cell operated in the dry coal syngas (Figure 3.2(b)), which indicated the formation of nickel phosphide. However, the Ni_3P^+ signal was very weak. Nickel phosphate was detected. In short, the degradation rate was accelerated by either applying the electrical current to the electrode or increasing the water content in the coal syngas. The applied electrical current in the wet coal syngas promoted the generation of nickel phosphate in the anode and loss of zirconia. The water content favored the formation of nickel phosphate, which deteriorated the catalytic activity and conductivity of the anode. After exposure to the dry syngas containing PH_3, nickel phosphate was not observed while nickel phosphide was detected in the anode.

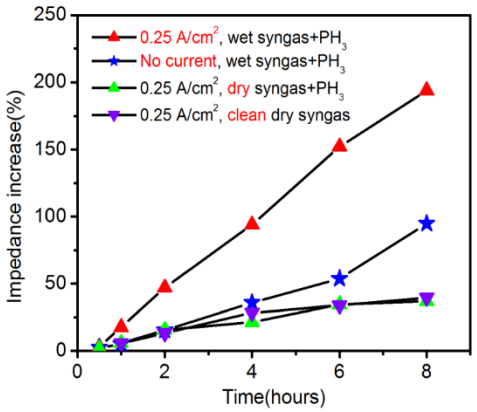

Figure 3.1: Polarization impedance increases as a function of operation time (5 ppm PH_3 at 800°C)

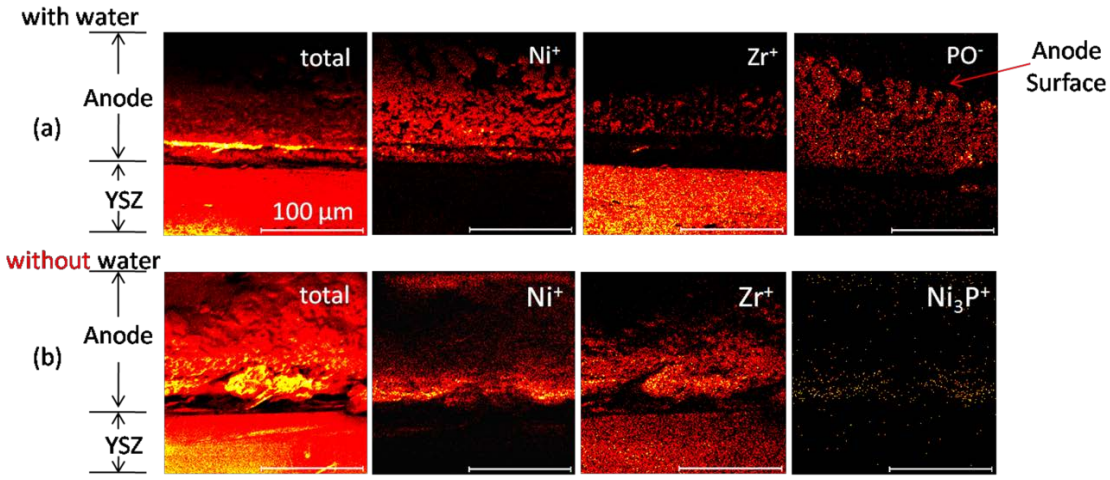

Figure 3.2: SIMS images of the cross-section of Ni/YSZ anodes after operated in 5 ppm PH_3 containing coal syngas for 24 hours at current density of 0.25 A/cm^2: (a) wet coal syngas, (b) dry coal syngas.

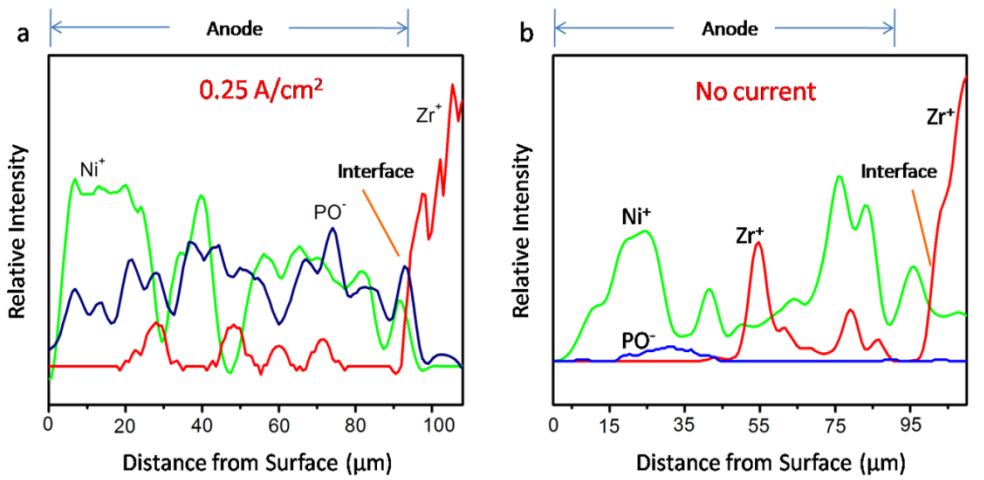

Figure 3.3: SIMS line analysis of the cross-section of Ni/YSZ anodes after operating in 5 ppm PH_3 containing wet coal syngas for 24 hours: (a) at current density of 0.25 A/cm^2, (b) without current load.

E-SEM is a useful tool for in-situ observation of the solid oxide fuel cell (SOFC) electrode. The E-SEM installed at WVU has the capability to heat the sample up to 1100^{o}C under vacuum. The morphology and

the phase contrast of the sample can be obtained by the secondary electron detector and bias control of metal plates above the hot sample. Figure 3.4 is a gold coated clean Ni-YSZ anode observed at 800 ^{o}C. The phase contrast suggests the interpretation of the bright dots as gold, the dark grey region as YSZ and the light grey region as Ni. While sputtered metal coatings are recommended for SEM samples with insulating materials, this image demonstrates the hazards of using a low melting and mobile conducting gold coating. More recently (see the appendix), the ESEM has confirmed the melting of nickel phosphide products on the surface of the anode between 900°C and 1000°C,

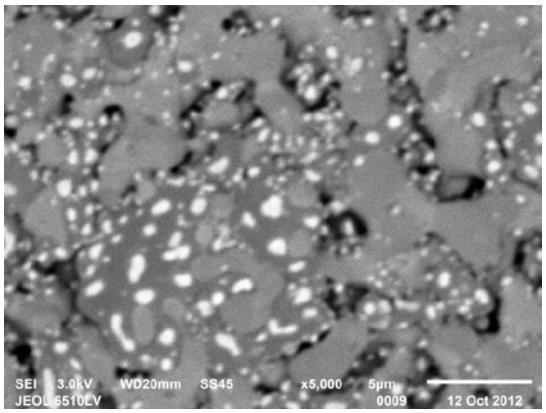

Figure 3.4: E-SEM image of a Ni-YSZ anode sample obtained at 800^{o}C

In order to determine the activation energy of the Ni-YSZ cermet, a patterned nickel micro-strip anode was fabricated using photolithography techniques. A 1 μm thick and 5 μm wide nickel layer was deposited on 8% Y_2O_3-stabilized ZrO_2 electrolyte. Figure 3.5(a) shows the schematic diagram of the electrode arrangement on YSZ electrolyte. This cell was tested under open circuit, 50mV, 100mV and 200mV overpotential in the temperature range from 700 to 800^{o}C (Figure 3.5(b)). The apparent activation energy was determined to be 0.88eV±0.04eV, which was comparable to the value reported previously in the literature. These results can be used to determine some unknown model parameters in the Butler-Volmer type equations.

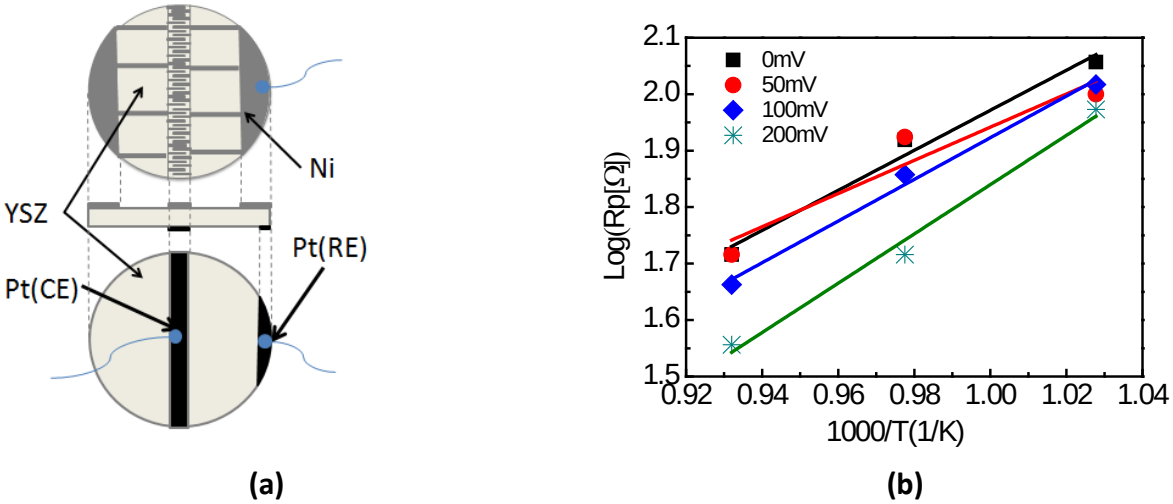

Figure 3.5: (a)Schematic diagram of the electrode arrangement on YSZ electrolyte, (b) Calculated activation energy under different over-potentials

3.2. Effect of the PH3 contamination on the microstructure

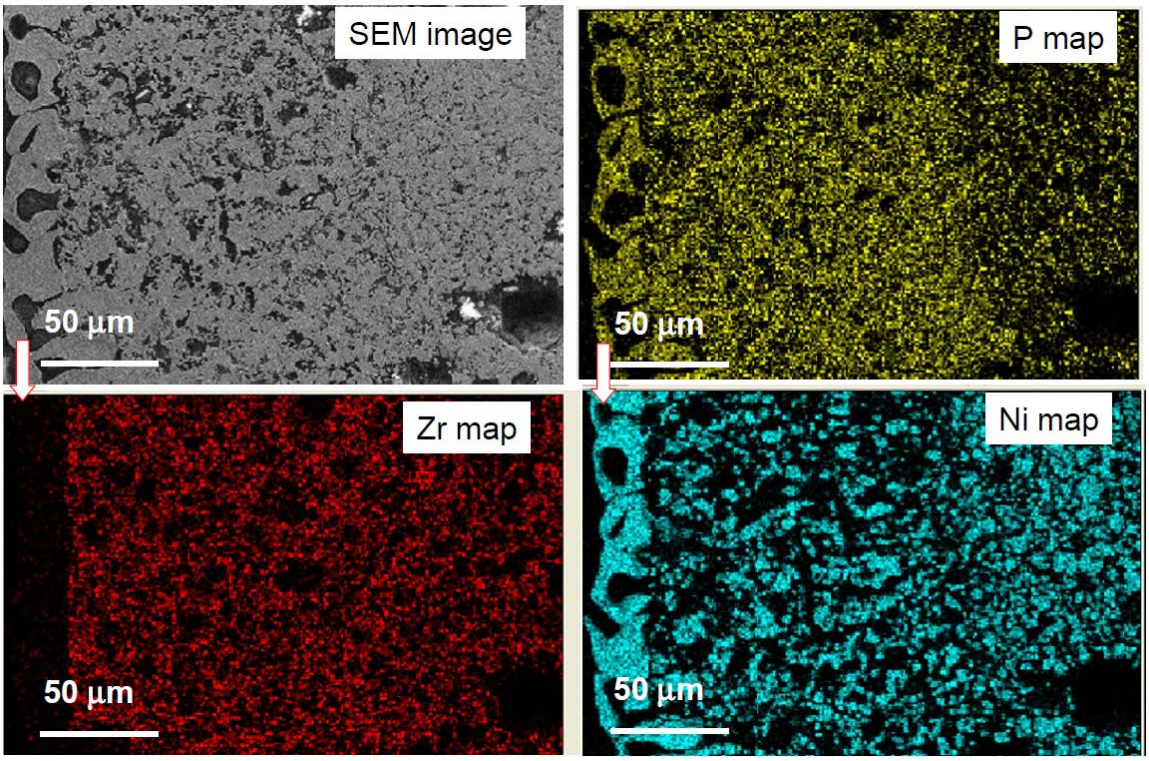

Figure 3.6: EDS mapping of external layer of the anode exposed to fuel with PH3

SEM imaging and EDS element mapping showed that the PH_3 exposure resulted in the formation of Ni-P phase on the external surface of the anode, as shown in Figure 3.6. The new nickel phosphide phase on the external surface of the anode is visible on the left side of each image. The chemistry of large scale Ni-P phase was also confirmed by EDS under TEM.

Detailed TEM analyses also showed that the external Ni-P layer is not a single phase, and that there are some precipitates (Figure 3.7) embedded in the main phase. The precipitates have some orientation relationship with the main phase.

The present work also demonstrated that PH_3 contamination affected the nanostructure and chemistry of YSZ electrolyte resulting in the possible formation of a YPO_4 phase (Figure 3.8) and the migration of Y dopants along the YSZ/Ni interfaces. A previously undetected YPO_4 phase was observed at the YSZ/YSZ/Ni triple grain junctions located at the interface with the YSZ electrolyte.

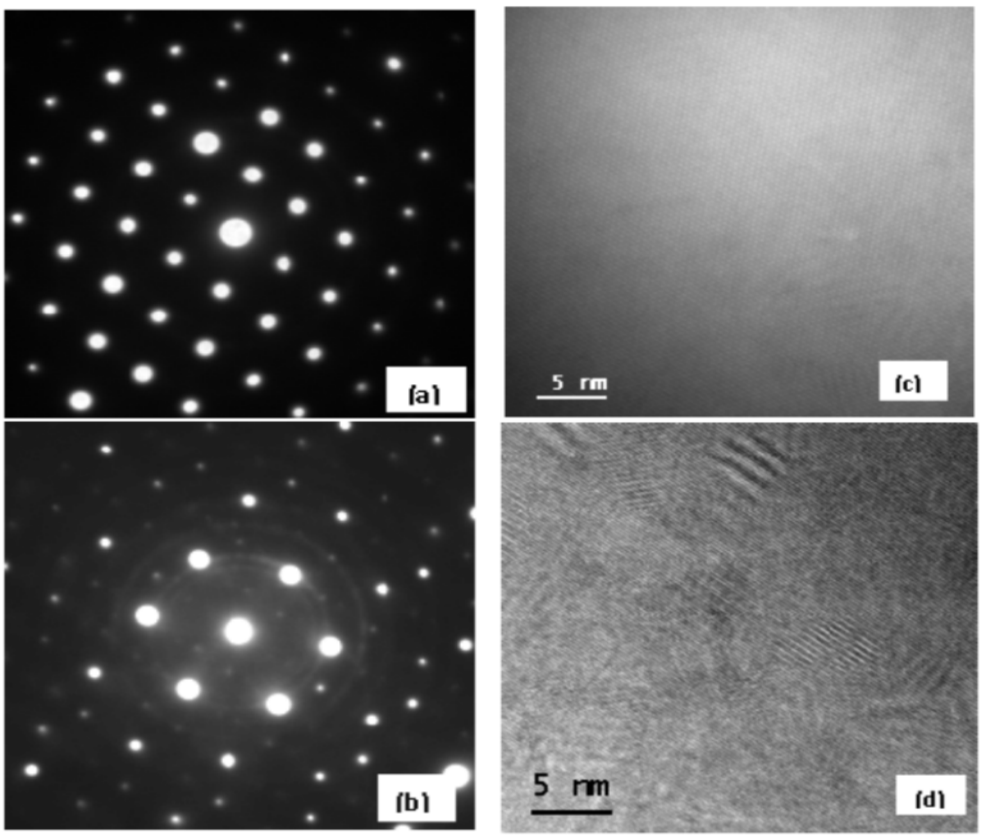

Figure 3.7: Presence of the precipitates in the Ni-P external layer.

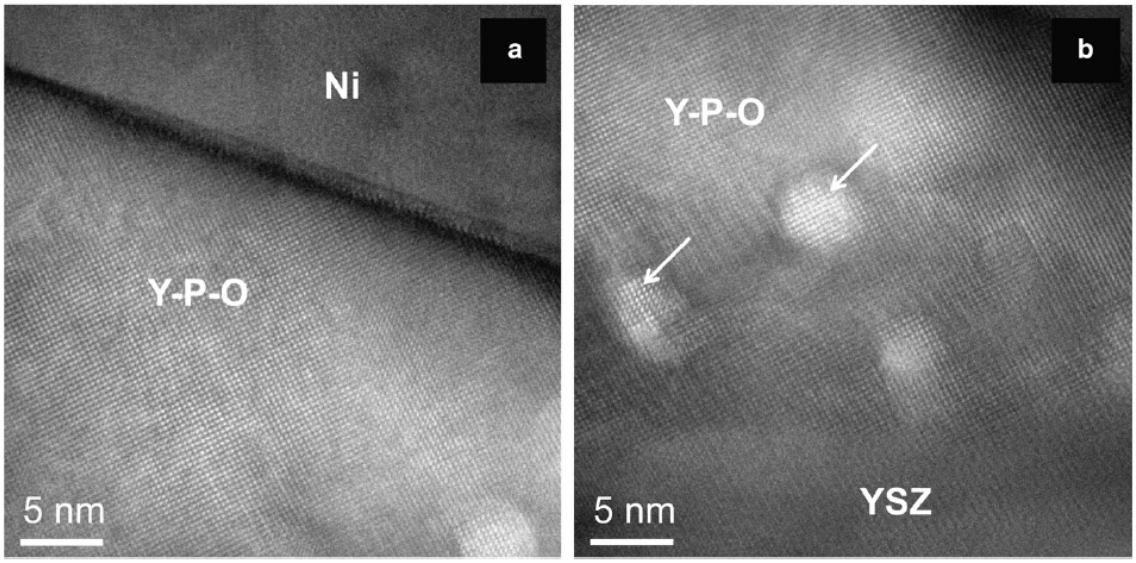

Figure 3.8: Formation of Y-P-O phase at the Ni/YSZ interface. Nano-scale YPO_4 phase was observed in the cell operated using the fuel of syngas with 10 ppm PH_3.

4. Mechanisms for H_2S degradation

The Ni-based cermet is a cost-effective SOFC anode material for hydrocarbon fuels; however, H_2S impurity in these fuels can cause degradation of cell performance by poisoning the Ni-based anode. Presvious studies have shown degradation of the performance of SOFCs when exposed to H_2S. At low ppm levels of H_2S the degradation appears to be reversible but at higher concentrations it is not. In an attempt to diminish or eliminate the deleterious effects of H_2S, SOFC's were produced in which a GDC barrier layer was incorporated on top of the traditional Ni-GDC anode structure. Nickel gadolinium doped ceria (Ni-GDC) hybrid anodes were exposed to synthesized syngas and H_2 fuels with various concentrations of H_2S at 800ºC under constant current conditions. The tests showed that the cells with a GDC barrier layer were resistant to H_2S impurities at concentrations up to 1000 ppm in wet H_2 and 100 ppm in syngas during long-term tests (Figure 4.1). Cells without the barrier layer had a significantly lower tolerance for the H_2S impurity. This result leads to the hypothesis that the GDC barrier layer assists in the prevention of nickel oxidation at the anode/electrolyte interface. Post-mortem analysis of the SOFC anode performed using SEM/EDS and XPS suggests that the mechanism of H_2S poisoning is not related to the formation of nickel sulfides on the anode.

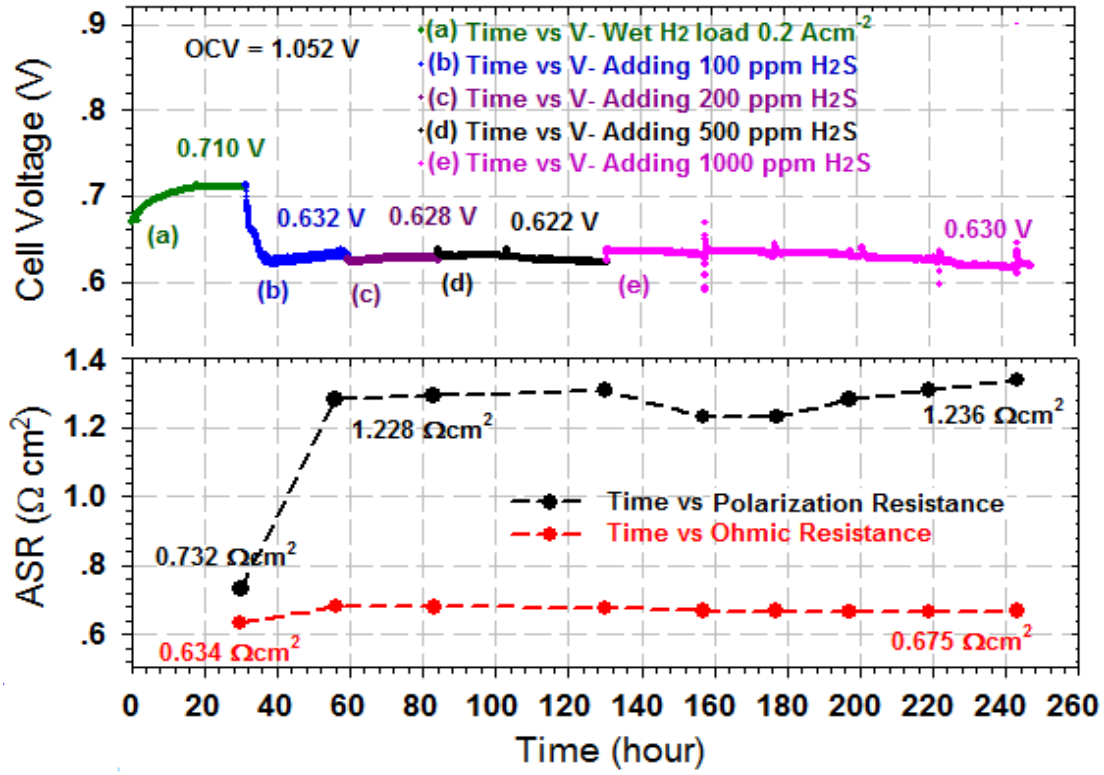

Figure 4.1: The cell voltage and ASR versus testing time of cell-6 (with the Ni-GDC-20 barrier layer in the anode).

A reference electrode was placed on the cells to monitor changes in the anode and cathode polarization resistances. The catalytic activity trend of yttrium chromites was explored by using a relatively complete doped yttrium chromite series. Materials with fairly good performance were obtained, providing an encouraging candidate for the H_2S-tolerant anode (Figure 4.2). Some findings from this study include:

a) Co or Ni at the B site is crucial to the catalytic property of the doped $YCrO_3$.

b) Without A site Ca doping, the performance in H_2 is relatively poor. A site elements can also alter the electrochemical activity of the catalyst by influencing the conductivity.

c) Good performance was obtained for YCCC. Polarization resistances of 0.85 and 0.5 Ω cm^2 were achieved on YSZ and SSZ electrolytes respectively.

d) The potential of using such materials as the cathode was also studied. A decent cathode performance was obtained for YCCC. In this case, if a symmetrical cell configuration is adopted using YCCC as both anode and cathode, the degradation from S poisoning can be possibly recovered by reversing the functionality of anode and cathode.

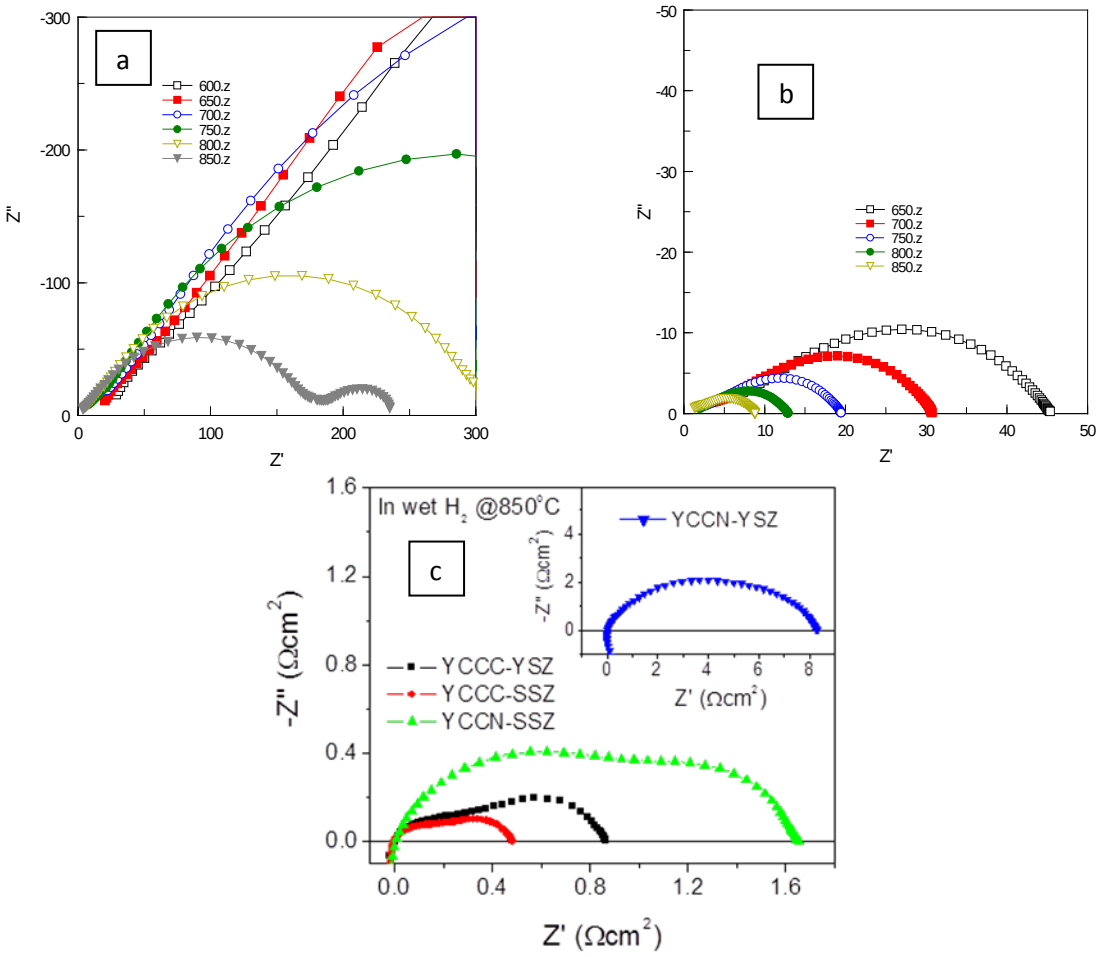

Figure 4.2: Performance of single phase YCC(a), $Y(CrCo)O_3$(b) on YSZ, and YCCC, YCCN(c) electrodes on YSZ and SSZ in 3% wet H_2 at different T.

5. Other Contaminants and Fuel

5.1. The effect of HCl in syngas on Ni–YSZ anode-supported solid oxide fuel cells

A 400-h test of a Ni–YSZ anode-supported SOFC cell exposed to syngas with 100 ppm HCl contamination was conducted. The degradation of cell performance (loss of voltage at constant current) was about 1.6% over the test period of 300 h at 800°C and 1.5% over 100 h at 850°C (Figure 5.1). The cell series and polarization resistances remained almost constant during 400 h of testing. The results indicated that the anode-supported cell has a higher tolerance for HCl impurity than the electrolyte-supported cell tested by previous investigators. The EDS data of the Ni–YSZ anode revealed that some loss of nickel concentration may occur due to attack of the Ni–YSZ anode by HCl over 400 h. Minor surface microstructural reconstruction of the Ni particles was observed in the SEM micrographs at 100K magnification. Traces of chlorine were found on the HCl-poisoned Ni–YSZ anode by XPS. The limited amount of Cl on the anode could be formed on the very surface of nickel particles by chemisorption processes at the SOFC working conditions. There was no evidence of the presence of nickel chloride compounds in the post-mortem Ni–YSZ anode. These findings suggest that the adsorption of chorine onto the surface of the Ni particles in the cell anode and the loss of nickel concentration are two related processes and both impact the cell performance. The loss of nickel was not significant in this study since the tests were conducted over only several hundred hours. However, it may have a more severe effect on the long-term durability of the SOFC power system, because it appears to be an irreversible process. The testing results also showed that 100ppm HCl can severely corrode stainless steel tubing. Clearly, HCl in syngas poses a challenge not only to the tubing but also to any interconnects based on stainless steel or other corrodible materials. This issue cannot be ignored in SOFC systems using coal syngas.

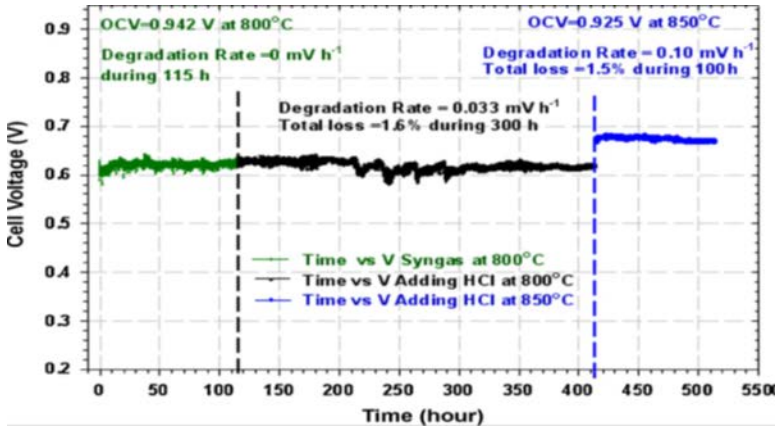

Figure 5.1: The cell was stabilized after exposure to clean syngas for 115 h, then 100ppm HCl was added for 400 h. The cell voltage drop is about 10mV in the first 300 h at 800°C, and 10mV in the next 100 h at 850 °C.

5.2. Tolerance tests of H_2S-laden biogas fuel on solid oxide fuel cells

Biogas is a potential source fuel for the SOFC by direct internal reforming (DIR) at the SOFC anode. It is a cheap and renewable fuel available from many sources, such as landfill gas, biomass, sewage, municipal waste, green waste and energy crops. The composition of biogas is a complex and variable mixture of CH_4 and CO_2 while containing a few percent of N_2, H_2, O_2 and trace contaminants such as H_2S, Cl_2 and F_2. Furthermore the Ni–YSZ anode with its "in situ" nickel catalyst and high operation temperature makes DIR of biogas possible. The internal dry (IDR), steam (ISR) and air with steam (IASR) reforming of clean biogas on an anode-supported SOFC (MSRI) was evaluated (see Figure 5.2). The basic barriers of implementing internal reforming of clean biogas are coking and differential thermal expansion by the

endothermic reforming reactions on the cell anode. It was found that the steam present in the reforming reactions (ISR) can largely reduce coking. Moreover, the endothermic reforming reactions were seen to cause severe cracks in the cell contacts and the cell anode. Introduction of the partial oxidation reforming reaction moderated the thermal effects from the endothermic reactions and minimized coking on the anode surface. The IASR case is one example of achieving the internal reforming of clean biogas on a SOFC. A Ni–CeO_2 coating layer applied to the anode was shown to improve biogas reforming without cracking and coking at 850 °C. The application of 20 ppm H_2S to the uncoated cell caused complete cell failure in very short time (see Figure 5.3). When 20 ppm H_2S is injected to the coated cell, the reduction of the biogas reforming on the Ni–YSZ anode was temporarily halted, but eventually this cell failed as well. However, nearly complete recovery of cell performance was noted after the H_2S was removed (see Figure 5.3). The major finding of this work was that the H_2S poisoning effects on the Ni–YSZ anode-supported SOFC are much more severe when using biogas fuel than for either H_2 or syngas fuel. The Ni–CeO_2 coating barrier can increase H_2S tolerance somewhat with lower degradation rate and high recoverability. Thus the application of Ni–CeO_2 coating presents a way to suppress coking and cracking while enhancing the resistance to sulfur attack for the Ni based anode.

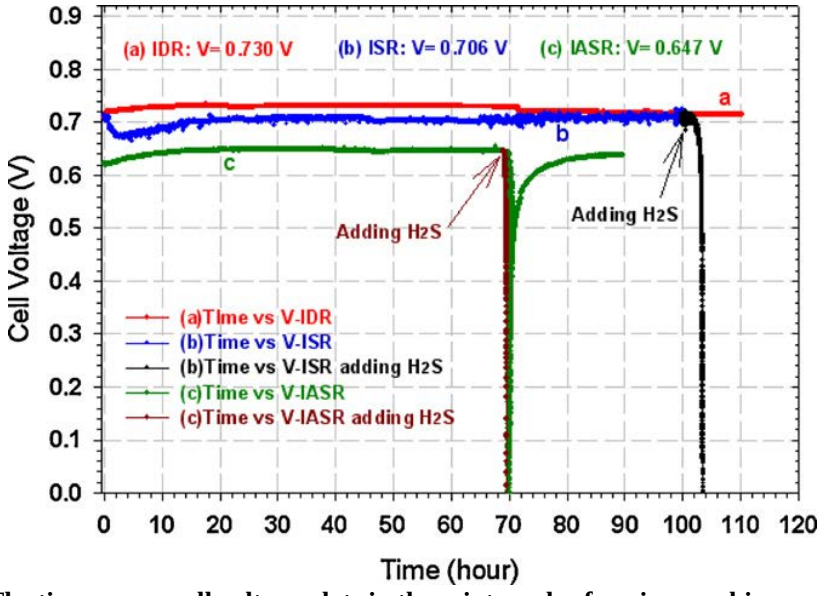

Figure 5.2: The time versus cell voltage plots in three internal reforming syn-biogas conditions. (a) Internal dry reforming (IDR). (b) Internal steam reforming (ISR) synbiogas and adding 20ppm H_2S for 3h. (c) Internal air with steam reforming (IASR) and adding 20ppm H_2S for 0.7 h.

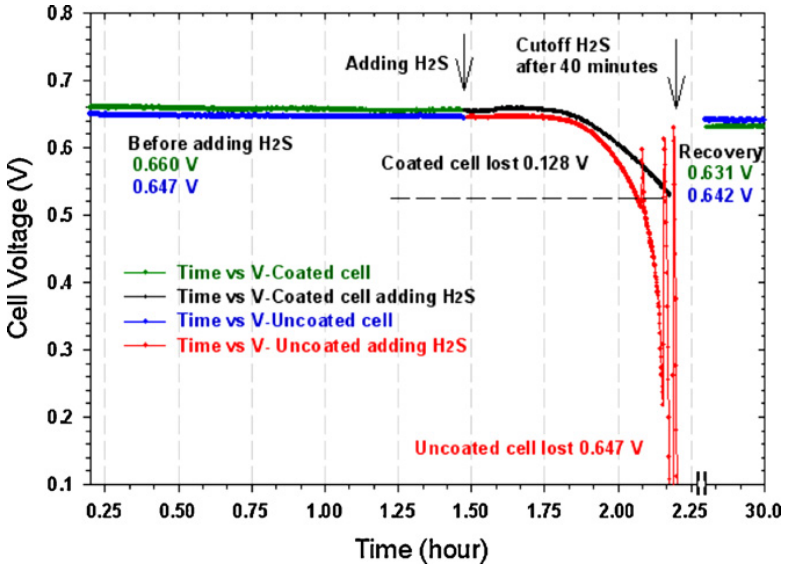

Figure 5.3: Comparison of the loss of voltage between the Ni–CeO_2 coated cell and uncoated cell after adding 20ppm H_2S impurity for 50 min in the second cycle (the time axis was adjusted for comparison).

5.3. Tolerance tests of co-feeding Cl_2 and H_2S impurities in biogas on a Ni-YSZ anode

In this aspect of the work, Ni-CeO_2 coated Ni-YSZ anode-supported cells were exposed to two different compositions of synthesized biogases (biogas) with 100 ppm Cl_2 under a constant current load at 850°C. The composition mole ratio of CH_4/CO_2 = 1.6 and 1.5 was used for internal steam reforming (ISR) and internal air with steam reforming (IASR) respectively. The electrochemical performance was evaluated periodically using standard electrochemical methods. Figure 5.4 shows the results for the ISR experiment with biogas and 100 ppm Cl_2. Over the course of nearly 200 hours in Cl_2, little degradation in performance was noted. Following the 200 hours in Cl_2, 20 ppm H_2S impurity was added to the fuel stream along with the Cl_2 impurity. The cell started to degrade and eventually lost all its performance. Interestingly, the experimental data in Figure 5.5 showed that 100 ppm Cl_2 impurity in the fuel gas can postpone but not prevent the degradation caused by addition of the H_2S impurity when compared to the degradation of H_2S alone. Thus the presence of Cl_2 in biogas can increase the tolerance of H_2S attack in the ISR case. This finding could lead the way to developing a chemical treatment to mitigate the poisoning effect of H_2S contaminant.

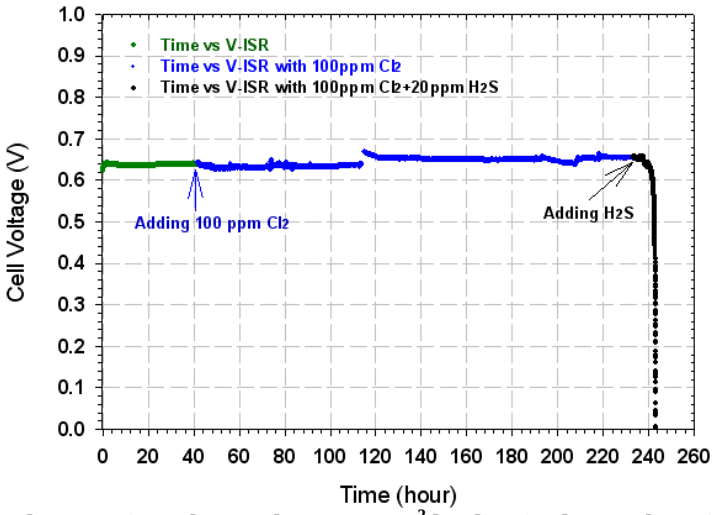

Figure 5.4: The cell voltage vs time plots under 0.5 A cm^{-2} loading in the ISR by using clean biogas fuel, adding 100 ppm Cl_2 in biogas and co-feeding 100 ppm Cl_2 and 20 ppm H_2S. The cell voltage dropped to zero in about 9 h.

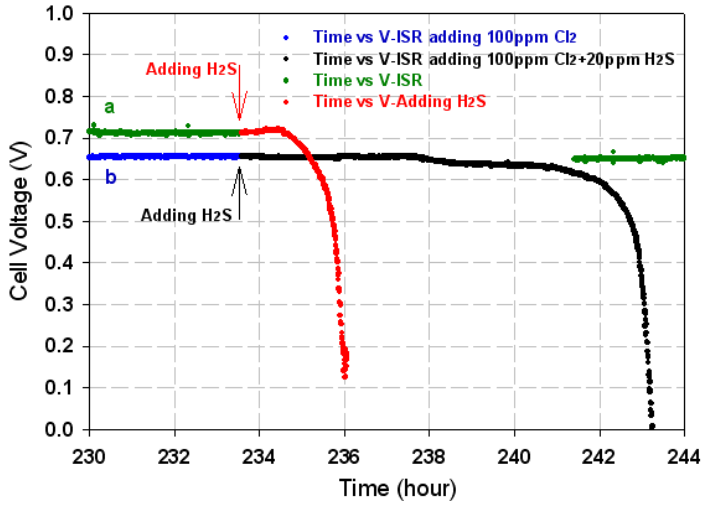

Figure 5.5: Comparison of the voltage loss between the addition of H_2S alone and co-feeding Cl_2 with H_2S contaminants in biogas for the ISR. The cell degradation in H_2S was postponed in the co-feeding case.

6. Remedies for Contaminant Effects

One of the aims of the EPSCoR project was to investigate methods by which the adverse effects of contaminants are reduced, hence increasing tolerance levels and the life time of the cells. Some of the remedies discovered are presented below in this section and in section 4 above.

6.1. LSM/GDC Bi-Layer

A porous, thin film of nickel tungstenate ($NiWO_4$) was screen-printed and subsequently bonded onto an yttrium-stabilized zirconia (YSZ) electrolyte-supported SOFC by treatment at 1000°C for 1 h. A bi-layer

composed of (La,Sr)MnO_3/ $Ce_{0.9}Gd_{0.1}O_2$ (LSM/GDC) was utilized as the cathode with the $NiWO_4$ composition acting as the sole anode for the SOFC. The ~1-cm diameter fuel cell with a ~100-µm thick YSZ electrolyte was tested in H_2 fuel at 800°C. During the insertion of the H_2 fuel, the $NiWO_4$ was reduced to form a Ni-WO_x cermet composite that consisted of a fine mixture of Ni-nanoparticles dispersed over the porous WO_x support structure. A reasonable maximum power density of ~104 $mW{\cdot}cm^{-2}$ was attained for the reduced $NiWO_4$ anode, even with an un-optimized and dense microstructure, on an electrolyte-supported cell. The power density was further increased to ~165 $mW{\cdot}cm^{-2}$ with the incorporation of GDC powder into the $NiWO_4$ anode. The same $NiWO_4$-GDC composite was tested within a fuel stream of H_2 containing 10 ppm PH_3. The cell demonstrated a degradation rate of 0.006 $V{\cdot}h^{-1}$ for 5 h at 750°C, which is similar to that observed for conventional Ni/YSZ cermets.

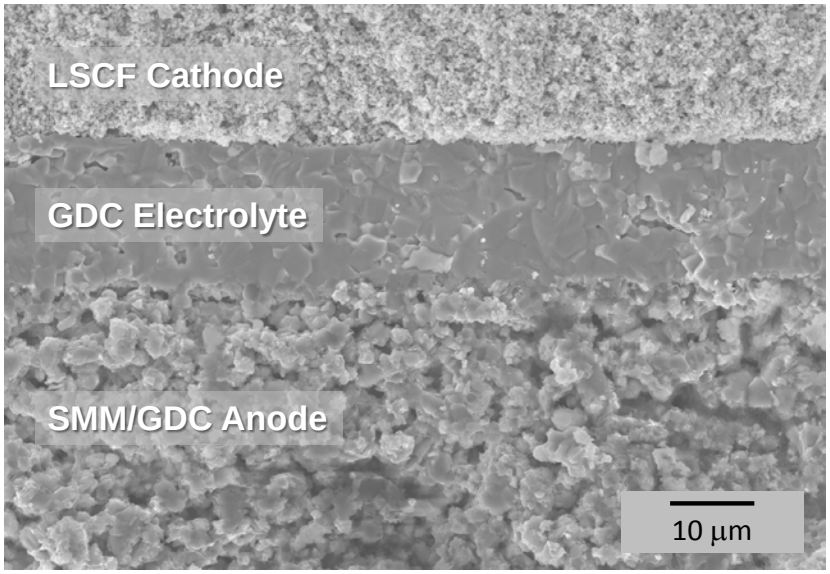

Figure 6.1: SEM micrograph of a SMM/GDC anode-support cross-section with the screen-printed GDC electrolyte after sintering.

6.2. SMM and GDC Anode

An anode-supported solid oxide fuel cell (SOFC) was fabricated using a porous composite of $Sr_2MgMoO_{6-\delta}$ (SMM) and $Gd_{0.1}Ce_{0.9}O_{1.95}$ (GDC) for the anode support (Figure 6.1). The electrolyte consisted of a 20 µm thick GDC layer, which was deposited by a combined screen-printing and sol-gel deposition processes. A porous $(La_{0.6}Sr_{0.4})_{0.98}$ $(Co_{0.2}$ $Fe_{0.8})O_{3-\delta}$ (LSCF) composition was used as the active cathode. Voltage-current-power (V-I-P) tests were completed on the cells in wet H_2, and the fuel cells displayed a maximum power density of 342 $mW{\cdot}cm^{-2}$ and 572 $mW{\cdot}cm^{-2}$ at 600°C and 700°C, respectively, without the use of any metal impregnate to enhance the electro-catalytic processes (Figure 6.2).

An all-ceramic solid-oxide fuel cell (SOFC) anode composed of a mixture of $Sr_2MgMoO_{6-\delta}$ (SMM) and $Ce_{0.9}Gd_{0.1}O_2$ (GDC) was synthesized and tested on zirconia electrolyte–supported SOFC's in clean and phosphine-contaminated hydrogen and coal syngas fuels. The SMM and GDC powders were prepared via solid-state reaction and co-precipitation, respectively. A 50/50 vol% homogenous composite of these two materials was synthesized and printed onto a GDC coated yttrium stabilized zirconia (YSZ) electrolyte support. The initial electrochemical performance of the cell at 800°C H_2 showed a maximum power

density of 290 $mWcm^{-2}$ and 180 $mWcm^{-2}$ in wet H_2 and in clean syngas, respectively. The same cell was tested in wet H_2 with 10 ppm PH_3, where the cell displayed stable performance over the first 40 h, but then slowly degraded over the next 80 h leading to a 47% decrease in power output (0.59%/h). Although the anode showed notable degradation over the 120 h test, the performance was much improved compared to that seen for typical Ni/YSZ cermet anodes where the anode failed within 30 h (Figure 6.2). Electron microscopy and x-ray photoelectron spectroscopy (XPS) were used to detect the possible mechanism(s) for this degradation. The XPS results did not detect P at the anode/electrolyte interface nor throughout the bulk of the anode in either a phosphide or phosphate form. Additionally, post-test analysis showed that the phosphorus did not react with any of the anode or electrolyte constituents. While still unclear, this initial work suggests that the degradation of the cell may be due to partial de-lamination of the cell at the anode/electrolyte interface.

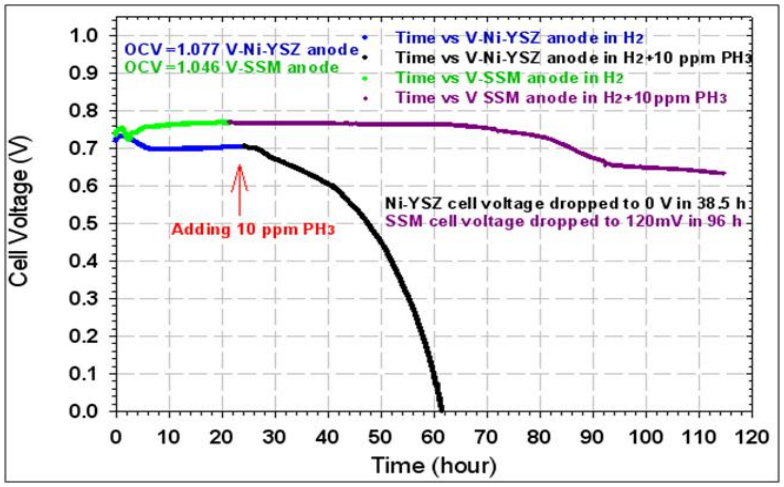

Figure 6.2: Comparison of the performance at constant current (0.25 Acm-2) in wet H2 adding 10 ppm PH3 between Ni-YSZ anode cell and SMM/GDC anode cell.

6.3. Removing PH_3 via a Ni-based Filter

Described here is a means of removing PH_3 impurity in syngas fuel by using a Ni-based filter. In one test, a thin Ni-based filter was set upstream of a Ni-YSZ anode-supported SOFC. The SOFC was exposed to syngas with PH_3 under a constant current load at 800°C. The filter effectively decreased 20 ppm PH_3 in the feed to a level which did not significantly degrade the SOFC for over 400 h until the filter became saturated (Figure 6.3). In another test, both H_2S and PH_3 were fed to the cell with Ni-based and Fe /Ni-based filters. The results showed that the interaction between these two impurities did not significantly impact the filter performance for both filter formulations. That is the filter was still capable of quantitatively removing the PH_3 even in the presence of the H_2S. But the cell showed the typical degradation behavior as seen earlier when H_2S was fed to the cell as the lone contaminant. The cell performance was evaluated by current-voltage measurements and impedance spectroscopy, in addition to thermodynamic and chemical analyses. The post-mortem analyses of the cell and filter were performed by means of XRD, SEM/EDS and XPS. With proper filter design, the Ni-YSZ SOFC can operate on contaminated coal-syngas without degradation over a prescribed period of time.

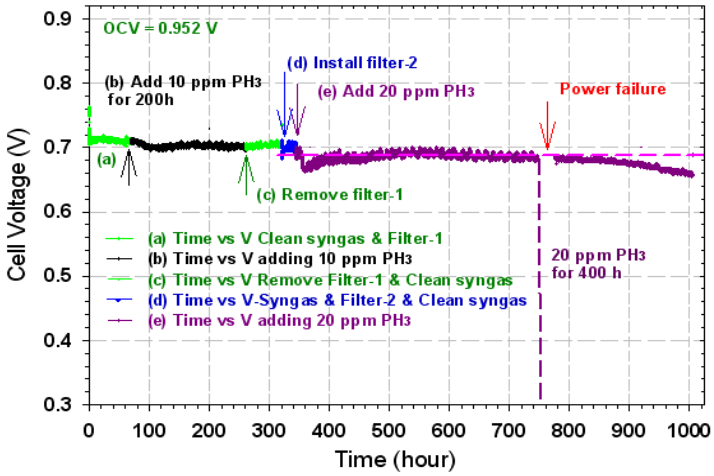

Figure 6.3: Cell voltage vs. time for a single SOFC with over 1000 hours of exposure to PH_3 in syngas.

7. Predictive Models for Performance Degradation

The objectives of this project are: (1) to develop a SOFC anode material durability model to predict the long-term thermo-mechanical behavior and fuel gas contaminants effects (As, P) on SOFCs and remaining service life, (2) to apply the durability model on a Planar SOFC for the prediction of long-term anode structural durability in an actual SOFC planar stack configuration, (3) to develop a computational model based on continuum hypothesis and execute this model to gain insight with regard to transport of critical species under realistic operating conditions for the anode as well as for a complete single cell and (4) to utilize the knowledge base obtained from accelerated cell tests at relatively higher concentrations of contaminants to develop theoretical models that could accurately predict the degradation behavior, life time and contaminant tolerance limits of cells operating on syngas with very low levels of impurities.

The major accomplishment of this project was the development of computational models to simulate SOFCs operating on coal syngas along with contaminant induced degradation. After extensive calibration and validation using button cell experiments, these models were used to predict the degradation patterns and life time of planar cells. In addition, simulation support was provided for experimental tasks in project 1 through equilibrium calculations and providing button cell temperature predictions for calibration of in-situ temperature measurements.

7.1. Thermo-mechanical degradation

We have identified several degradation mechanisms such as thermal stresses, thermal aging, redox cycle, and coal syngas impurities that may degrade SOFC anode structural properties during long-term operation. An anode durability model was developed that incorporated thermo-mechanical and fuel gas contaminants (P, As, etc.) effects on the anode microstructure. The model was implemented in finite element analysis to predict anode structure durability. Figure 7.1 shows time evolution of percentage of the two modes of degradation at the center of anode. It is seen as the time increases the contaminant degradation becomes more dominant.

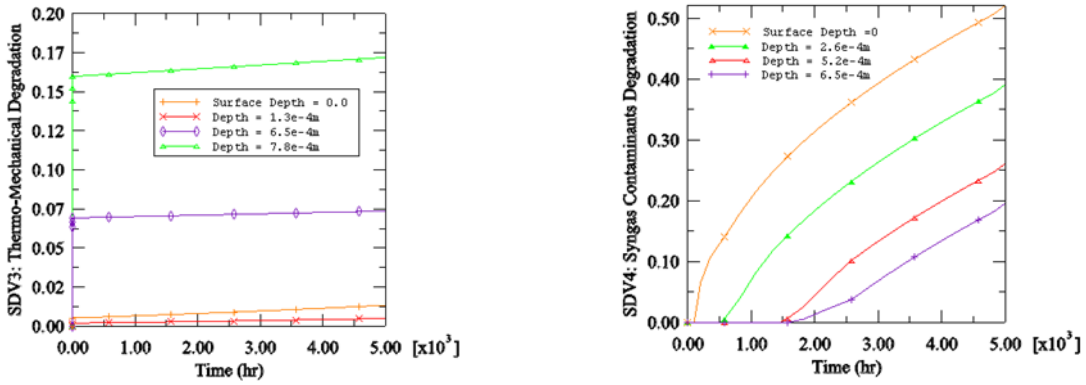

Figure 7.1. (a) Evolution of percentage of thermo-mechanical and (b) syngas contaminants degradation within anode thickness at the center during 5000hr of exposure to 5ppm of phosphorus

The anode structural durability model, which incorporated thermo-mechanical and fuel contaminants effects, was enhanced to predict the long-term structural behavior of a planar-SOFC anode. The temperature field and contaminant concentration distribution on the SOFC anode are required inputs for the model that are deduced from DREAM-SOFC: a multi-physics code for SOFC modeling developed in house. The cumulative effect on the anode structure due to the two degradation mechanisms is assumed to be multiplicative. Since anode material behaves as elastic brittle material from room to the operating temperature, the critical degradation value is taken to be 0.4.

Figure 7.2 shows the predicted evolution of the cumulative degradation at the anode exposed surface. Initially the cumulative degradation is dominant at the fuel inlet and propagates along the fuel flow largely due to the contaminant structural degradation. Gradually the thermo-mechanical degradation effect increases at the anode/electrolyte interface near the fuel outlet and propagates towards the fuel inlet. In the long run, the two degradation effects concentrate at the anode exposed surface and the cumulative degradation variable reaches its critical value near the mid-section of the anode depending on the operating temperature and contaminant concentration.

Co-flow, counter-flow and cross-flow configurations are distinguished according the relative flow directions of fuel and air on the anode and cathode respectively. In order to understand the anode structure degradation for the three configurations, cell-temperature fields and contaminant distributions are implemented in the model to predict the anode structural degradation under similar operating conditions.

The model predicts that the co-flow arrangement yields the longest anode structural life as compared to the other two configurations under similar operating conditions as shown in Figure 7.2. In co-flow configuration, thermo-mechanical degradation is severe at the fuel outlet and contaminant degradation starts near the fuel inlet, whereas in other configurations, thermo-mechanical and contaminant degradations start near the fuel inlet regions. The current general view is that the cell electrochemical degradation is the dominant factor that dictates SOFC working life when working under coal syngas. These conclusions are derived from accelerated exposure tests performed under much higher concentration of fuel contaminants. Consequentially, the cell electrochemical performance decreases to an unacceptable level in a short period of time before there is any measurable structural degradation. However, as indicated in Figure 7.3, under lower PH_3 concentrations the anode structure degradation may be significant as compared to its electrochemical degradation.

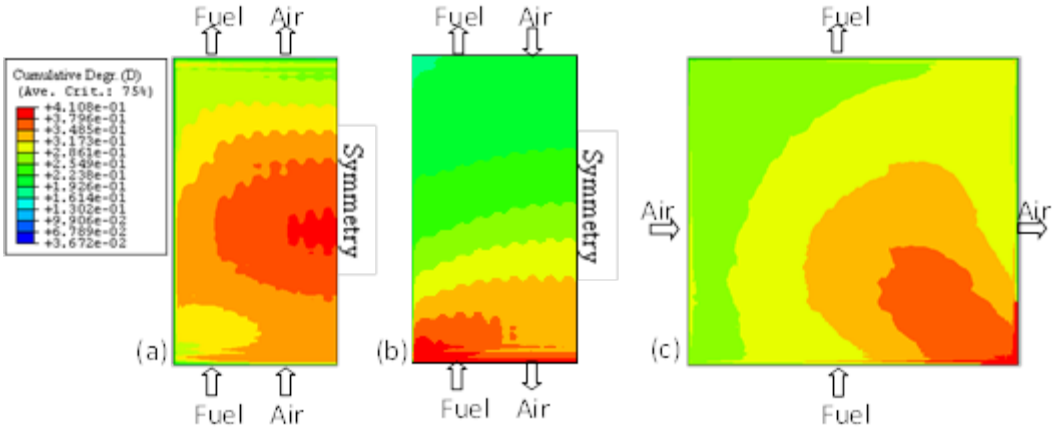

Figure 7.2: Anode structure failure locations comparison (a) co-flow:19920h (b) counter-flow:16310h (c) cross-flow: 18450h

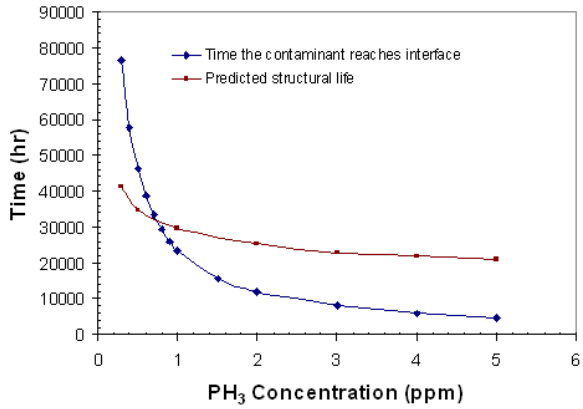

Figure 7.3: Comparison of predicted anode structural life and time required to reach to interface

7.2. Electro-chemical degradation model

7.2.1 Computational Model for SOFCs Operating on Hydrocarbon Fuels

A detailed computational model for simulating SOFCs operating on a variety hydrocarbon fuel mixture was developed using an existing model that could only handle hydrogen fuel. This task required formulating and implementing in the existing computer code, several sub models which include: multi-component mass transfer, electrochemistry with simultaneous oxidation of hydrogen and carbon monoxide, bulk reaction chemistry and surface reaction chemistry. In our study, it was found that, when applied to mass transport modeling in a SOFC anode, the errors (compared to a more accurate dusty gas model) in simple Fick's model, which is commonly used in SOFC modeling, increased with the cell current; reaching unacceptably high values at high currents. As a remedy a correction was formulated and calibrated for the effective multi-component diffusion coefficient such that Fick's model produced same results as the dusty gas model even at high cell currents. This approach for multi-component diffusion fluxes was successfully adopted in the subsequent modeling studies.

A broader electrochemistry model is formulated to account for simultaneous electrochemical oxidation of CO and H_2 both of which could be electrochemically active under SOFC operating conditions. The challenge was to estimate the effective cell voltage when these two fuels with different heating values are producing current in parallel and to find the contribution of each of these to the total cell current. The expanded electrochemistry sub-model adeptly addressed these issues and the resultant SOFC simulations

yielded noteworthy results regarding the contributions from CO and H_2 electrochemistry to the total current produced by the cell.

Three different reaction mechanisms, with varying degrees of complexity, were implemented to account for the bulk reactions of hydrocarbon fuels occurring inside the anode such as water gas shift (WGS) and Methane Steam Reforming (MSR): (i) A two reaction model developed for catalytic methane reforming, (ii) an Augmented Reduced Mechanism, and (iii) a detailed surface mechanism with 42 reactions and 18 species which could also model the catalytic effect of Ni in the anode. The three mechanisms were compared against each other in terms of predictions of key parameters, detailed additional information produced, and computational cost. The two reaction model is chosen for majority of subsequent simulations with the other two mechanisms used in only limited simulations due to high computational costs.

The computational model is calibrated against numerical results from literature. Simulations are performed using the model to predict performance of button cells tested under Project 1. A good agreement was obtained between the measured and simulated VI curves. In addition the model was used to calibrate the unique in-situ temperature measurements performed under Project 1.

7.2.2 Fuel Contaminant Induced Degradation Model

A novel phenomenological mathematical model is formulated to simulate the transport and reaction of fuel impurities inside the SOFC anode with the goal of capturing the typical degradation pattern observed for contaminants such as P and As where the deposition of the impurity on the Ni catalyst starts near the gas stream/anode interface and slowly moves toward the active anode/electrolyte interface. The model parameters are calibrated to match the degradation rates reported by PNNL. The model parameters were calibrated to match the experimental degradation rates reported in literature for impurities such as arsine (AsH_3), phosphine (PH_3), hydrogen sulfide (H_2S) and hydrogen selenide (H_2Se) using only one accelerated test case; all the other cases are predicted with the same parameters. The results at various temperatures and contaminant concentrations agree well with the experiments (see Figure 7.4 and Figure 7.5).

Using the calibrated model, predictions are made for different contaminant levels and correlations are obtained for anode life time versus the contaminant concentration (see Figure 7.4 b where all symbols represent simulations not experiments.). These correlations enable the determination of expected cell life time for very low contaminant concentrations as well as the tolerance limit for a specific contaminant in order to achieve a prescribed anode cell life time. In addition simulations are performed for simultaneous exposure to multiple contaminants. Several strategies were employed to account for combined effect of different secondary species formed due to multiple contaminants. All the simulations show that the degradation rate of cells exposed to multiple contaminants is faster than that of cells exposed to any one of the contaminants.

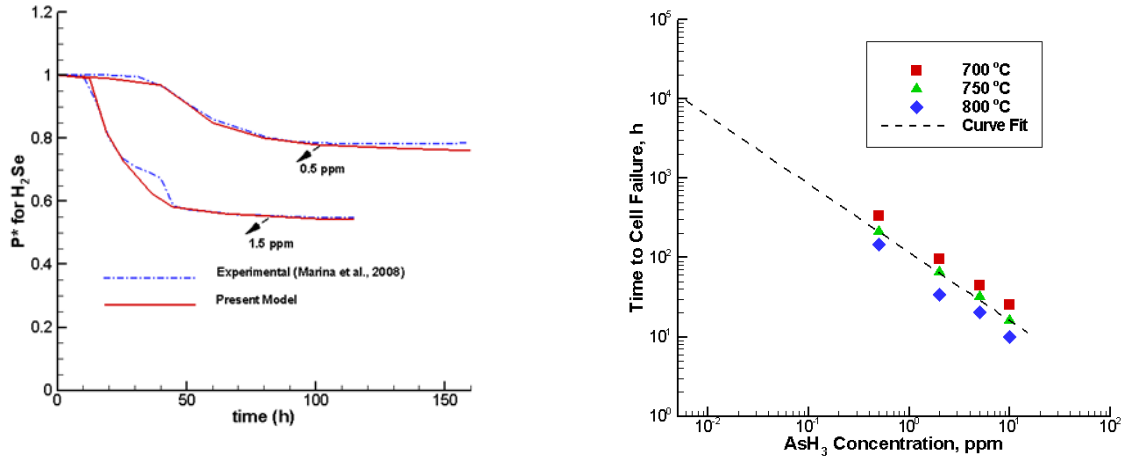

(a) **(b)**

Figure 7.4: (a) Calibration of modified power density against experimental data adopted from Marina *et al.* (2008) for 1.5 ppm H_2Se in coal syngas at 800 °C (b) Time to cell failure for electrolyte-supported cells exposed to simulated coal syngas with varying concentrations of arsine at different operating temperatures

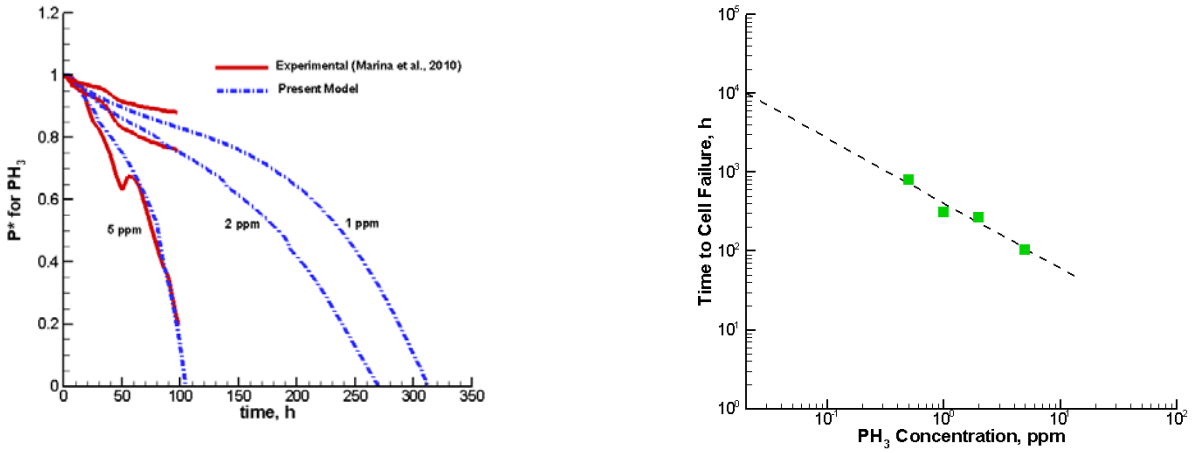

(a) **(b)**

Figure 7.5: (a) Validation of the calibrated phosphine degradation model for concentration effect (b) Time to cell failure for electrolyte-supported cells exposed to simulated coal syngas with varying concentrations of phosphine at 800 °C

The model was also further improved to emulate the experimentally observed dependence of the degradation rates in cells exposed to PH_3 on the water vapor content in the fuel. Based on the observation that different Ni-P secondary species are formed under wet and dry fuel conditions, the model equation that relates the local contaminant coverage to porosity is also made function of water content in the fuel. With this modification, the sensitivity of degradation rate to water content is accurately predicted in agreement with experiments.

7.2.3 Equilibrium Computations

Gas phase and multi-phase equilibrium calculations were performed to aid experiments in identifying the possible stable forms of the impurities under SOFC operating conditions. A large database of thermo

chemical properties of possible coal syngas components and their derivatives in the SOFC environment was compiled in order to perform the equilibrium calculations. Equilibrium calculations were performed to identify the most stable forms, both in gaseous and condensed phases, in which phosphorous may occur under SOFC operating conditions for various initial phosphorous concentrations and at different temperatures. It was found that P_2O_3 is the major phosphorous species under such conditions. These findings were used to analyze the experimental results for P contaminant obtained under Project 1.

Further, novel transient simulations are performed using equilibrium calculations to predict the amount of Ni conversion to secondary phases when exposed to PH_3. The methodology involves equilibrating the amount of Ni present in the SOFC anode with the amount of gas that passes through the anode in a certain time interval. The new state of solid phase with some condensed secondary phases of P formed with Ni is then taken as new initial condition and equilibrium calculations are repeated with a new batch of fresh fuel mixture. The time evolution of Ni conversion could thus be obtained by repeating these iterations. The computations predict that Ni_2P_5 was the major secondary species that forms whereas experimental results have shown that other phosphides or even phosphates could also be present. In addition, the rate of Ni conversion predicted by this model increased with the impurity concentration, cell operating temperature and pressure which is also observed in the experiments.

7.2.4 Planar Cell Simulations with degradation

Large planar cells operating on coal syngas were also simulated using the in-house modeling code DREAM SOFC. Simulations are performed for both coal syngas and partially reformed methane fuel. It was shown that when operating on methane fuel, a careful thermal management is required to avoid detrimental temperature gradients inside the cell.

Finally, the calibrated phenomenological model for contaminant induced degradation is incorporated into the 3D SOFC modeling code DREAM SOFC. This effort is the culmination of all the previous work and it combined knowledge and insights from the tasks performed thus far to produce unique predictions of contaminant induce degradation trends inside large industrial scale planar SOFCs. Simulations are performed for a planar cell operating on hydrogen fuel with PH_3 impurity using the model parameters determined from button cell simulations. The results show that the contaminant coverage of Nickel distribution inside the anode is highly non-uniform. These non-uniform distributions are caused by the geometrical alignment of gas channels and current collectors, as well as the variation of gas concentration along the flow direction. The non-uniform deactivation of anode gave raise to altering of current distribution inside the planar cell such that the cell can still produce current even when some regions of the anode are partially inactive (see Figure 7.6a). This is in stark contrast with what is observed in button cells where all the distributions are essentially one-dimensional. The degree of non-uniformity in the deactivation profiles is a function of the relative magnitudes of diffusion and reaction time scales. Predicted V-I curves of the planar cells at different stages of degradation show that the cell failure is hastened by a decrease in the cell limiting current upon exposure to PH_3 while the activation losses are mostly unaffected (See Figure 7.6b).

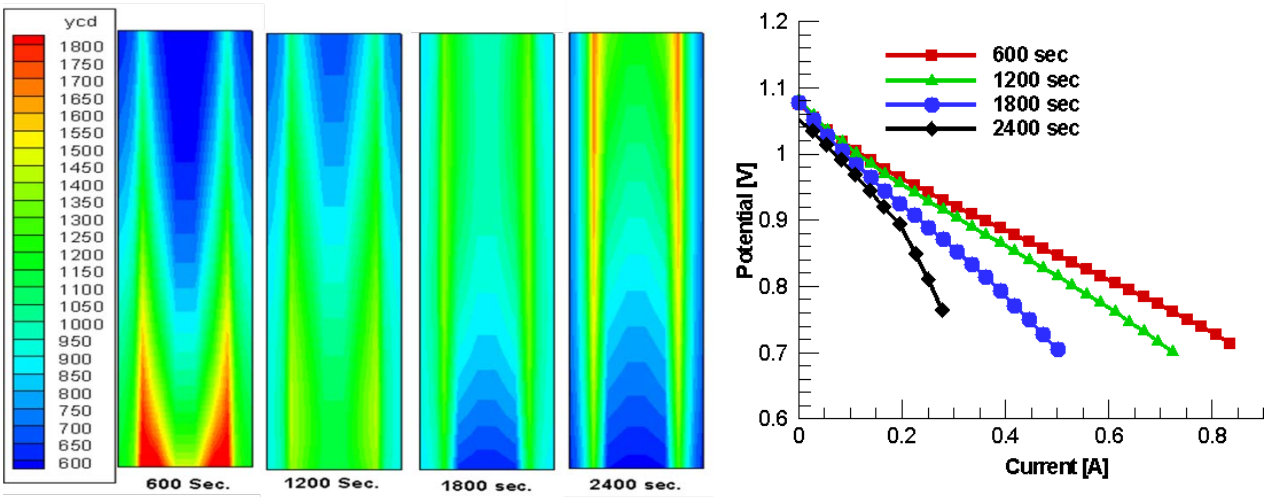

Figure 7.6 : (a) Current density distribution at the anode/electrolyte active interface of a co-flow planar cell (only one channel of the cell is simulated) operating at 0.1 A/cm^2 current density at different times after exposure to 50 ppm PH_3 (b) Predicted VI curves for a planar cell operating at 0.1 A/cm^2 current density at different times after exposure to 50 ppm PH_3

Conclusions

The main focus of this project has been the effects of PH_3 on SOFC anodes, especially the widely used Ni/YSZ anode. While consistent results were not obtained, the general trends of SOFC performance shows a slow loss or no loss for a brief period when ppm levels of PH_3 are present in "dry" hydrogen, and more rapid loss and sometimes rapid failure in humidified hydrogen and syngas. Current flow exacerbates the degradation rate. Mass spectroscopic analysis of exhaust gases confirms that PH_3 reaches the anode in "dry" hydrogen and that thermodynamically predicted products of PH_3 at high temperatures do not survive in this environment. Despite the absence of visible reaction products of PH_3 in humidified fuels, a variety of post-mortem analysis clearly reveal the presence of phosphorus as nickel compounds on and in the anode. There is also evidence for the reaction of the YSZ electrolyte with the phosphorus species. No remedy other than the use of a reactive filter ahead of the anode has been found for the deleterious effects of PH_3. Simulation models have been developed using both these results and literature results to provide predictions of degradation patterns and lifetimes in both button cells and flow cells with parallel gas flows.

The modeling approach uses accelerated tests on small button cells for calibration of the model parameters, then it is applied to larger cells and stacks with more realistic geometry and operating conditions.

As for infrastructure and work force building, the WVU team has been very successful in terms of recruiting new faculty, training many postdocs and students in the area of fuel cell technology. Using the experience gained, the members of the research team have secured significant amounts of external funding from agencies such as NETL/RUA, SECA, ARPA-E, DOE-EE and DOE-FE in the same and related areas. Particularly the new Center for Electrochemical Energy Storage Systems (CEES) lead by Dr. X. Liu will benefit greatly from the infrastructure build and the experience gamed under the EPSCoR Project.

References

[1] Cayan F.N., Zhi M., Pakalapati S.R., Celik I., Wu N., Gemmen R., Effects of Coal Syngas Contaminants on SOFC Anodes: A Review, Journal of Power Sources, 183, 2008

[2] Zhi M., Chen X., Finklea H., Celik I., Wu N. Q., Electrochemical and Microstructural Analysis of Ni-Yttria Stabilized Zirconia Electrode Operated in Phosphorus-Containing Syngas, Journal of Power Sources, 183, 2008

[3] Marina O. A., Pederson L. A., Coyle C. A., Thomsen E. C., Edwards D .J., Nguyen C. D. and Coffey G. W. (2008), Interactions of Ni/YSZ Anodes with Coal Gas Contaminants, 9th Annual SECA Workshop, Aug 7, 2008, Pittsburgh, PA.

[4] J.W. Stevenson, O.A. Marina, C.A. Coyle, and D.J. Edwards, "Effects of Phosphorus and Arsenic on SOFC Anodes," 12 th Annual SECA Workshop, 2011

Acknowledgement

This work is conducted under US DOE (Department of Energy) EPSCoR Program. It is jointly sponsored by US DOE Office of Basic Energy Sciences, NETL (National Energy Technology Laboratory), WV State EPSCoR Office and the West Virginia University under grant number DE-FG02-06ER46299. Dr. Tim Fitzsimmons is the DOE Technical Monitor. Dr. R. Bajura is the Administrative Manager and Dr. I. Celik is the Technical Manager and the Principal Investigator of this project.

Appendix A

A.1. Accomplishments in Fiscal Year 2013-2014

Our overall research work conducted under the EPSCoR program is divided into three major sub topics namely; (i) Characterization of contaminant effects, (ii) Continuum level modeling, (iii) Anode material development and cell testing. In what follows we report on accomplishments in the last year, 2013-2014, with no cost extension.

A.2. Project 1: Characterization of Contaminant Effects

A.2.1. Project Objectives

Phosphine causes degradation of Ni/YSZ anodes when it is present in the fuel at ppm levels. The rate of degradation appears to correlate with the presence or absence of water in the fuel mixture. Previous studies have also shown that the new phase that appears on the anode surface can either be nickel phosphides (reduced phosphorus) or nickel phosphates (oxidized phosphorus). Consequently, there are questions on the nature of the phosphorus species reaching the anode as a function of the fuel composition.

The first objective of this sub-project is to use a mass spectrometer to determine the fate of phosphine in "dry" and "wet" hydrogen mixtures as a function of temperature of the gas mixture and the presence or absence of a Ni/YSZ anode in an operating SOFC. The second objective is to use the environmental mass spectrometer to examine the structures and morphologies of electrode structures as a function of temperature, from room temperature to 1100ºC.

A.2.2. Accomplishments

In last year's report, experiments were described of temperature studies with gases flowing through alumina tubes, with and without pieces of Ni/YSZ present. The gases were passed through an alumina tube or through a Probostat unit (also with alumina tubes) and the exhaust gases were analyzed with a Cirrus MKS mass spectrometer (mass range 1-100). In "dry" H_2, phosphine (PH_3, ~20 ppm) reacted to form undetectable products at temperatures between 400ºC and 600ºC. Above 600ºC, PH_3 exited the hot zone unscathed. Clearly, PH_3 would reach the anode of a SOFC in a "dry" H_2 mixture. In "wet" H_2 (~10 torr H_2O), PH_3 appeared to react nearly quantitatively at all temperatures above 300ºC. The temperature profile of the O_2 signal tracked the temperature profile of the PH_3 signal, suggesting that oxygen is a co-reactant. No products of the reaction were observed by mass spectroscopy. In particular, products predicted by thermodynamic data (HPO, HPO_2 and HPO_3) were not detected. In the presence of a piece of NiO/YSZ and "dry" or "wet" H_2, the PH_3 signal was reduced to low levels after the NiO was reduced to Ni, and remained at low levels until the temperature was reduced close to room temperature.

A.2.3. Summary of this year's observations

Since reaction products of PH_3 were not detected, the products formed either were non-volatile (depositing on the walls of the alumina tube) or possessed a mass outside the range of the mass spectrometer. The role of alumina in the reaction was checked by repeating the experiments using a quartz tube. The same pattern of reactivity was observed: (a) reaction of PH_3 at intermediate

temperatures (400-600ºC) in "dry" hydrogen; (b) reaction of PH_3 at temperatures above 300ºC in "wet" hydrogen; (c) no detectable reaction products. Alumina is not affecting the reactivity of PH_3.

An operating SOFC (Ni/YSZ anode, YSZ electrolyte, LSM/YSZ cathode) was mounted in the Probostat with the cathode exposed to flowing air and the anode to a fuel mixture of either "dry" or "wet" hydrogen, with and without 20 ppm PH_3. The mass spectrometer analyzed the fuel gas exiting the Probostat. The mass spectrometry data was used to confirm the formation of a gas tight seal between the anode and cathode sides of the SOFC and to monitor the reduction of NiO to Ni.

An example of one test is shown in Figure 1.1 (left) (signals at mass 28 (N_2) and mass 32 (O_2)), and Figure 1.1 (right) (signals at mass 18 (H_2O) and mass 34 (PH_3)). Note that all signals except mass 28 are not calibrated.

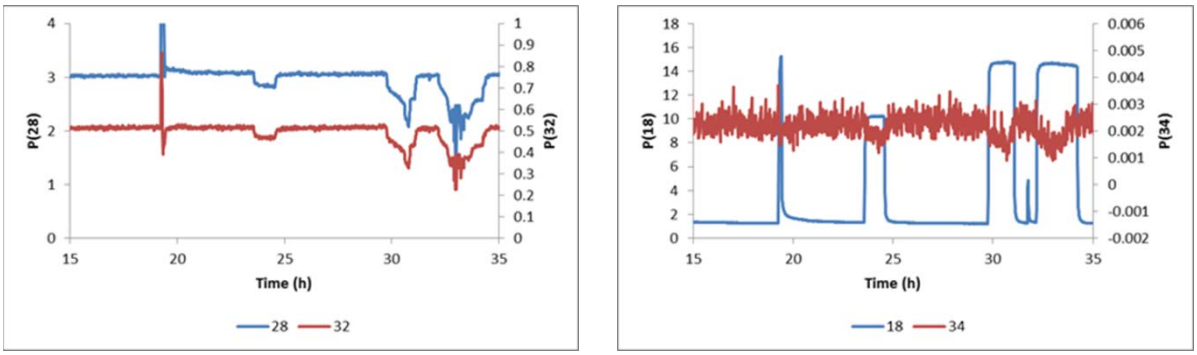

Figure 1.1: Mass 28 and mass 32 signals vs time (left); Mass 18 and mass 34 signals vs time (right)

At 19 hours, PH_3 (20 ppm) was added to "dry" H_2 while the cell was at OCV. The spikes in all gas signals were caused by residual air in the gas manifold line for PH_3. The mass 34 signal did not change, indicating that PH_3 did not survive the trip to the anode and back to the exhaust. At 24, 30 and 32 hours, the cell voltage was set at 0.9 V, 0.7 V and 0.5 V. Oxidation of H_2 yielded large increases in the mass 18 signal as expected. The dips in mass 28 and mass 32 signals are due to displacement of N_2 and O_2 by H_2O. The slight dips in the mass 34 signal are attributed to the same cause. The residual signal at mass 34 is assigned to oxygen 34 with a natural abundance of 0.4% of the oxygen 32 signal.

During all operating conditions, the mass 34 signal for PH_3 remained at the residual level, and no products of PH_3 oxidation were detected in the mass range of 45-100. A post mortem analysis of the SOFC showed the presence of a new crystalline phase on the external surface of the anode rich in nickel and phosphorus. XRD analysis indicated that the new phase was Ni_5P_2.

Subsequent experiments with a YSZ plate as a blank and without any plate in the Probostat showed that PH_3 was generated inside the Probostat at 800ºC in "dry" hydrogen with no added PH_3. Addition of water, dilution of the hydrogen with helium, and lower operating temperatures all resulted in sharply reduced or negligible PH_3 signals. The prolonged exposure of the alumina tubes to PH_3 at high temperature (~30 accumulative hours), with and without H_2O, appeared to have left a contaminant inside the tubes. This contaminant reacted with H2 at high temperatures to generate PH_3. Repeated attempts to remove the contaminant using washes with cold water, hot water and acetone, and scrubbing of accessible parts reduced the PH3 signal but did not eliminate it. The nature of the contaminant is not known, since phosphorous oxides and oxyacids are highly soluble in water and should be easily removed by aqueous washes.

The JEOL Environmental Scanning Electron Microscope (ESEM) with the Gatan hot stage is capable of generating images of samples under vacuum at temperatures up to 1100ºC. The sample stage consists of a platinum cup with a surrounding heater, and aperture plates above the sample to minimize radiative heat to the ESEM optics.

Temperature study of a Ni/YSZ plate after exposure to PH3

A Ni/YSZ piece was exposed to PH_3 in "dry" H_2 for 96 hours. The sample was imaged without the presence of a conducting layer; thermal emission of electrons at high temperatures reduces charging effects. At room temperature and at 800ºC, an array of particles with dimensions of 10 microns were visible on the surface of the Ni/YSZ (Figure 1.2). The shape and size of the particles were stable for at least 10 hours at 800ºC. Between 900ºC and 1000ºC, the particles melted, and they re-solidified at 800ºC (Figure 1.3). Since nickel phosphide phases have substantially lower melting points than nickel or nickel phosphates, the melting behavior suggests that the particles are a nickel phosphide phase.

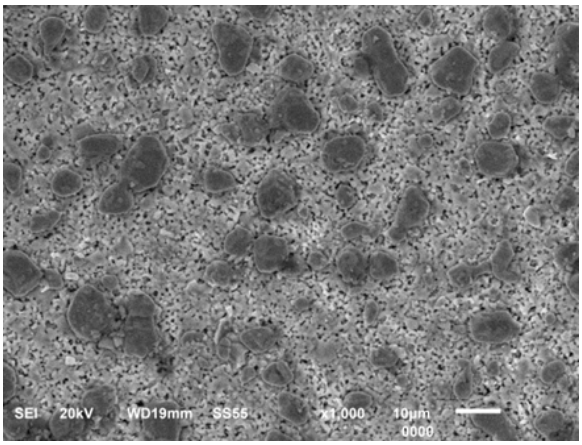

Figure 1.2: Image of the Ni/YSZ surface at 800ºC.

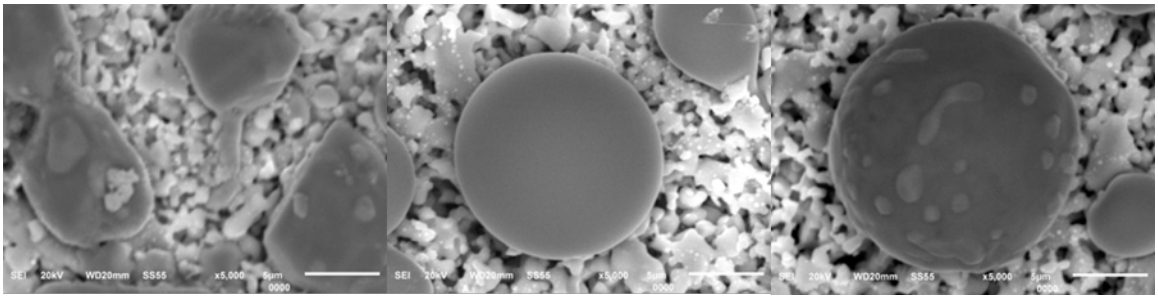

Figure 1.3: Image of the Ni/YSZ surface at 900ºC (left), 1000ºC (middle) and 800ºC (right).

Temperature study of LSM on YSZ

This experiment is not directly related to the project goals but is of interest to SOFC researchers. Gorte and co-workers (J. Electrochem. Soc. 2009, 156, B602) reported that LSM particles in YSZ single crystals undergo visible changes in shape at 1000ºC and are invisible at 1250ºC. In this experiment, a thin layer of LSM powder was applied to a YSZ substrate and sintered at 1200ºC. The sample was

sputtered with gold and imaged at temperatures up to 1080ºC. Within the resolution of the ESEM, the LSM particles showed no visible changes in morphology or size (Figure 1.4).

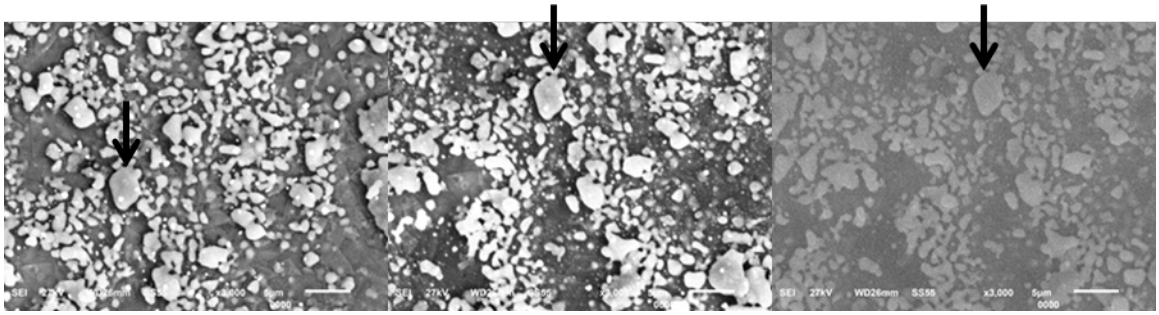

Figure 1.4: LSM particles on YSZ at 900ºC (left), 1000ºC (middle), and 1080ºC (right). Detector saturation resulted in poor image contrast above 1000ºC. The arrows indicate the same particle in each image.

A.3. Project 2: Continuum Level Modeling

A.3.1. Project objectives

The main objective of this study is to predict induced by impurities found in coal syngas degradation patterns in the SOFCs anode. The major accomplishment during the last year of this project are: (1) Validation of the 3D degradation model (DREAM-SOFC) using PNNL experiments (2) prediction of the electrochemical behavior of the planar SOFC anode exposed to phosphine at any given degradation stage, (3) formulation and application of a nickel migration model for SOFC is operating under phosphine exposure.

A.3.2. Description of accomplishments

A three dimensional code developed in house, (DREAM SOFC) which is capable of simulating the performance of SOFCs operating with a variety of fuel mixtures was enhanced to simulate the performance degradation of anode supported planar cell due to phosphine contaminant in hydrogen. In what follows a brief description of code is given:

DREAM SOFC's calculations are based on a cell level model which includes current collectors, anode, electrolyte, cathode, gas and fuel channels. Temperature distribution is solved for each component of the cell. The mass transport of gas species is solved along the gas channels, inside the porous anode and cathode. The specie coverage on active nickel sites is calculated using a transport equation similar to the one dimensional degradation model. The charge transport equations are solved for the entire cell. Electrochemical reactions are solved for both CO and H_2. The code is capable of simulating a mixture of CO and H_2, H_2O and N_2 on the fuel side and O_2 and N_2 on the cathode side. The empirical parameters of contaminant degradation model for planar cell were first calibrated using the one dimensional model to investigate the experimentally observed degradation patterns. The three-dimensional degradation model (DREAM-SOFC) is validated using PNNL's flow by anode contaminant tests. Further, simulations were performed for a planar cell operating on hydrogen fuel with PH_3 impurity and additional simulations were performed to predict the electrochemical behavior of the degraded cell at any given degradation stage. Finally, a transport model for nickel migration is formulated based on experimental observations. This model is integrated with an in-house one dimensional code for predicting SOFC anode degradation due to fuel impurities.

A.3.3. Accomplishments

Simulation of PNNL Experiments

SOFC anode performance degradation caused by fuel contaminants is altered by operating conditions (Temperature, current load and fuel utilization) and fuel composition (contaminant concentrations). In this section, an attempt is made to simulate anode contaminant test that was performed at Pacific Northwest National Laboratory (PNNL)[4]. Operating conditions, fuel concentrations, cell geometry parameters and calibrated degradation model parameters are listed in Table 2.1. The fuel utilization that is given in Table 2.1 corresponds to 0.8 A/cm^2 current density. Both the experiments and simulations were performed at open circuit voltage (OCV). The cell is modeled in 3D along 5.08 cm long fuel channel and through a 50/50 vol% Ni/YSZ 500 microns thick anode with 40% porosity. Simulations were performed with two different mass transfer coefficients of contaminant from fuel channel to porous anode. The degradation model parameters for 1ppm AsH_3 in utilized fuel containing %55 H_2 and 45 % H_2O were taken from previous work.

Table 2.1: Model parameters used for AsH_3 degradation and test conditions for the PNNL experiments

Geometry Parameters of the planar SOFC		**Conditions and parameters for simulation**	
Anode thickness	500 µm	Fuel inlet composition (Mole fractions)	55% H_2 + 45%CO_2+ 1ppm ASH_3
Electrolyte thickness	20 µm		
Cathode thickness	10 µm	Fuel inlet temperature (K)	1073
Fuel channel height	2.5 mm	Current density (A/cm2)	0
Air Channel height	2.5 mm	Fuel Utilization (%)	65
Cell length	5.08 cm	Anode porosity	0.48
Current collector width	1.27 cm	Mass transfer coefficient of contaminant	Case 1: 1e-5
Channel width	2.54 cm		Case 2: 1e-6

It is assumed that the secondary phases can be represented by the trace element coverage. Therefore, for the comparison between experiment and simulations, the normalized coverage profiles which are extracted from the simulations are used. As it is seen in Figure 2.1 simulations by DREAM-SOFC show good agreement with the PNNL experiment. In both simulations and EDS analysis, the arsine nickel interaction near the surface is much higher than the regions far from the surface. The simulation with lower arsine mass transfer coefficient shows a better agreement with experiment than that of higher mass transfer coefficient. This parameter is difficult to determine either experimentally or theoretically, while the mass transfer from the channel to the porous electrode is altered significantly as secondary phases form and change the morphology of the electrode surface. Simulations and experimental analysis indicate that, for fuels contain low contaminant concentrations (≤1 ppm), trace element coverage can still occur, but the low rate of contaminant propagation can significantly reduce performance degradation rates of SOFCs anode.

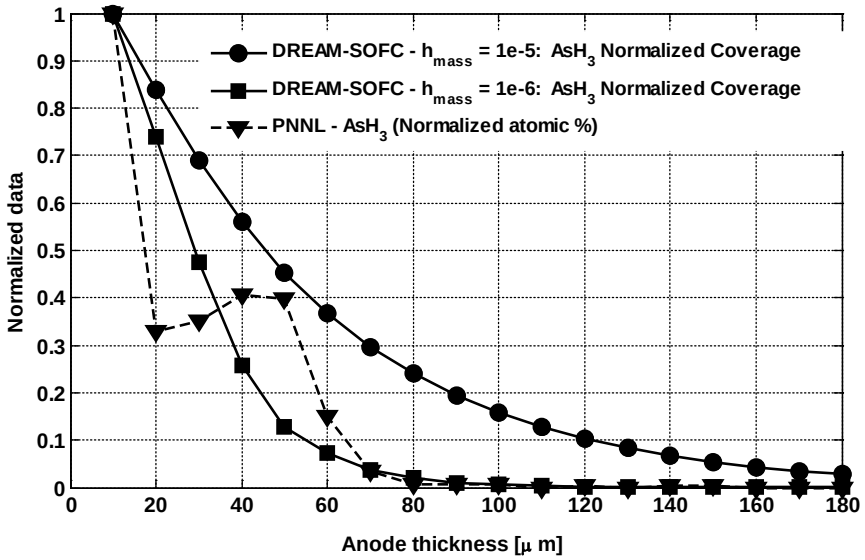

Figure 2.1: Normalized atomic concentrations profiles at 50 hours of arsine exposure from EDS analyses by PNNL and normalized arsine coverage at 50 hours of arsine exposure from simulations performed with two different arsine mass transfer coefficients ($h_{mass} = 1e-5$ and $1e-6$) from fuel channel to porous anode

Phosphine Induced Degradation in a Planar SOFC

The detailed geometric parameters and operation conditions used for the current simulations are given in Table 2.2. This cell represents closely the one used in the parallel experimental study by Drs. Sabolsky and Zondlo. A mixture of hydrogen, steam and phosphine was supplied to the anode side, and air was supplied to the cathode side. The computational domain is chosen such that it represents a practical repeat unit, containing one air and one fuel channel, in a planar cell of length 5cm. The choice of the computational domain thus makes the simulations more manageable in terms of computer time and memory while providing accurate predictions for a representative repeat unit of the cell. Figure 2.2(left) shows the predicted history of voltage produced by the cell operating at 0.1 A/cm^2 with dry hydrogen containing 10 ppm PH_3. Initially there is a slight increase in the cell voltage as the cell temperature increases due to heat produced inside the cell. After that there is a steady state behavior until phosphine exposure starts. Once anode is exposed to phosphine, the cell starts to loose performance due to the phosphine exposure.

The voltage drops by 32 % within 6.4 hours. Beyond that time the simulation became unstable due to instabilities in hydrogen transport equation. These instabilities exist due to the decrease in the hydrogen diffusion coefficient, which is altered by the impurity coverage. The coverage variation at a monitor point in the anode active layer, after phosphine exposure is shown in Figure 2.2 (right). Figure 2.3 and Figure 2. 4 show the distribution of hydrogen and oxygen mass fractions, respectively, at different stage of the degradation process. Initially, hydrogen is being consumed near the inlet. As the porosity and the activity changes by increasing nickel deactivation and secondary phase formation, utilization near the inlet decreases and shifts downstream. This, in turn, causes redistribution of oxygen on the cathode side.

Table 2.2: Geometry and operating conditions parameters for planar SOFC

Geometry Parameters of the planar SOFC		Conditions and parameters for simulation	
Anode thickness	50 µm	Fuel inlet composition	99.99% H2 + 10ppm PH3
Electrolyte thickness	170 µm	(Mole fractions)	
Cathode thickness	50 µm	Fuel inlet temperature (K)	1073
Fuel channel height	2.5 mm	Air inlet Composition (Mole fractions)	21% O2
Air Channel height	2.5 mm	Current density (A/cm2)	0.1
Cell length	5 cm	Fuel and air Utilizations (%)	12.5 and 1.25
Current collector width	1.28 mm	Anode porosity	0.48
Channel width	3 mm	Cathode porosity	0.45

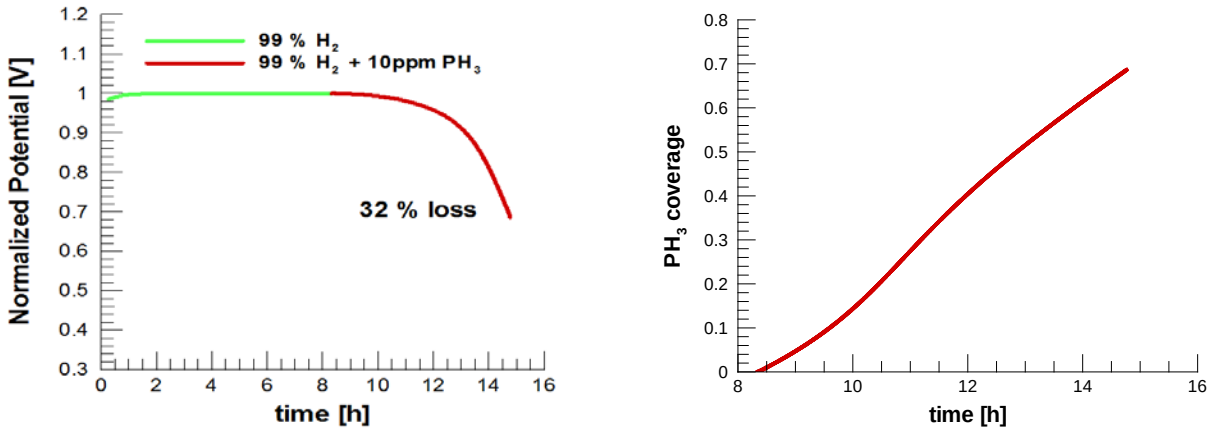

Figure 2.2: Cell voltage drop (left) and phosphine coverage formation at electrolyte/anode interface (right) during phosphine induced performance degradation

The anode regions directly underneath the inlet region are initially exposed to the phosphine introduced in the fuel and the active nickel sites in that region are thus consumed first by phosphine attack. This can be seen from contours of PH_3 coverage at anode/electrolyte active interface in Figure 2.5 for three different degradation stages. It is seen that the PH_3 coverage in the regions underneath the inlet region is much higher compared to that in the regions near the outlet and the coverage is also increasing with time. As the coverage of PH_3 builds up near the active interface it reduces the electrochemical activity of those regions. In addition the coverage also decreases (by design of the model) the porosity of the affected regions and reduces the effective gas diffusion coefficient. The local charge transfer kinetic is thus altered by the PH_3 coverage and the current distribution inside the cell changes with time as coverage distribution evolves with time. Figure 2.6 shows the current density distribution at the active anode/electrolyte interface at four different stages. It can be seen from Figure 2.6 that during the initial stages there is relatively high charge transfer rates in the regions underneath the channel inlet, but as the electrochemical activity is diminished due to contaminant coverage, the current densities in this region are reduced. Consequently, in order to maintain the applied constant average current density, the current is redistributed and the local current densities increased with time in the regions underneath the ribs and channel outlet. This redistribution, however, is not sustainable since the regions underneath the rib are hard to replenish the reactants especially when the effective gas diffusivity in the regions underneath the channel is lowered due to contaminant coverage. These simulations were performed before experiments which are described in section 3.

As depicted in Figure 2.3, the hydrogen is also re-distributed at the anode/electrolyte interface as the degradation progresses. The simulation thus becomes unstable (indicative of cell malfunctioning) when insufficient reactants are available in the regions where there is high electrochemical activity. In the current simulations the occurrence of insufficient reactants is handled by re-scaling the electrochemical potential in the starving computational cells using the ratio of available hydrogen to hydrogen required for the predicted charge transfer rate in the cell. In reality, however, the oscillations observed in current simulations could also mean that the cell experiences a catastrophic failure about the time at which the oscillations have started. In a real cell, if some regions become starved of hydrogen, the charge transfer redistributes to other regions. But in the current simulations, the regions where hydrogen is available are electrochemically inactive (due to contaminant coverage) and thus the cell may not be able to produce the applied current causing the voltage to drop suddenly.

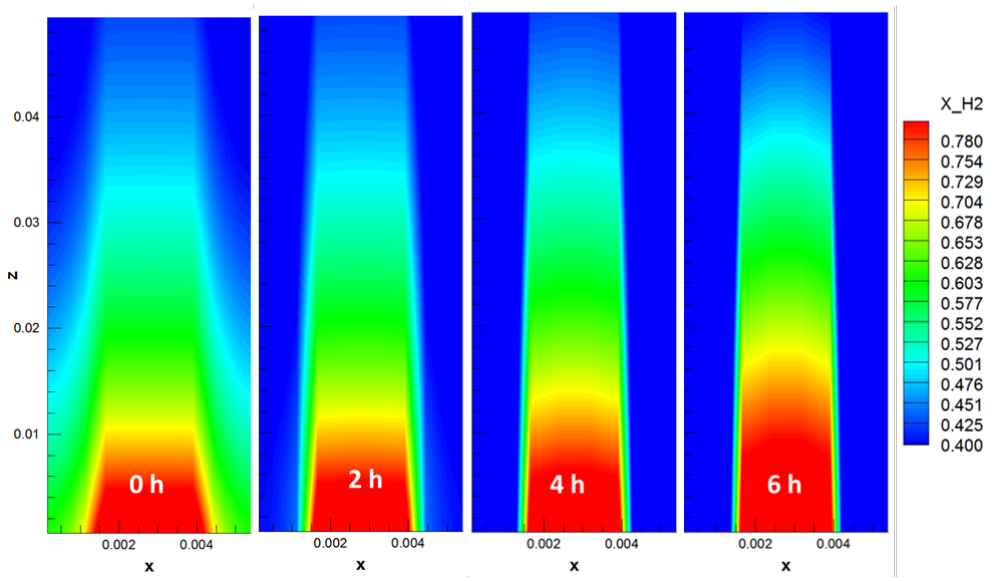

Figure 2.3: Contours of hydrogen mass fraction at cathode/electrolyte interface at steady state (top-left) after 2 hours (top-right), 4 hours (bottom-left) and 6 hours (bottom-right) of phosphine exposure

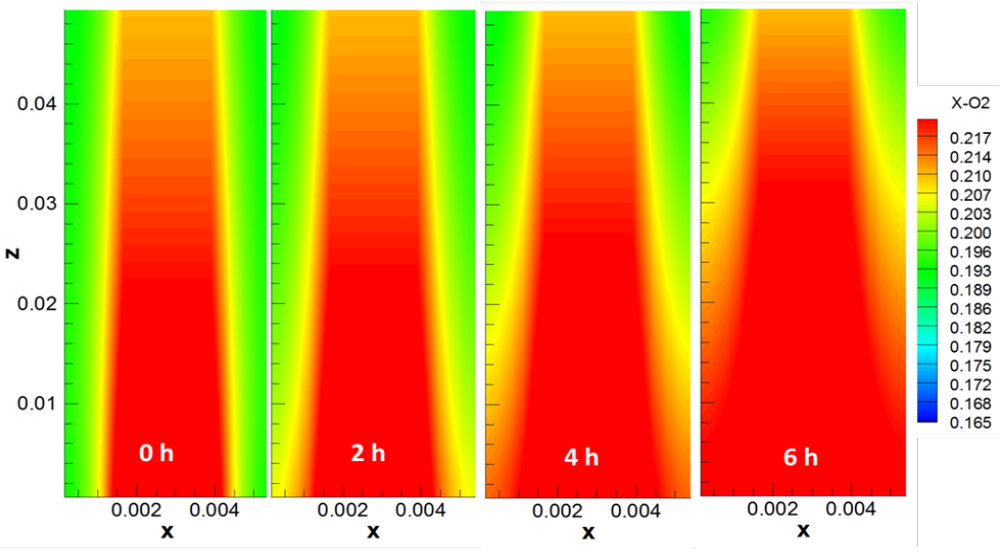

Figure 2. 4: Contours of oxygen mass fraction at cathode/electrolyte interface at steady state (top-left) after 2 hours (top-right), 4 hours (bottom-left) and 6 hours (bottom-right) of phosphine exposure

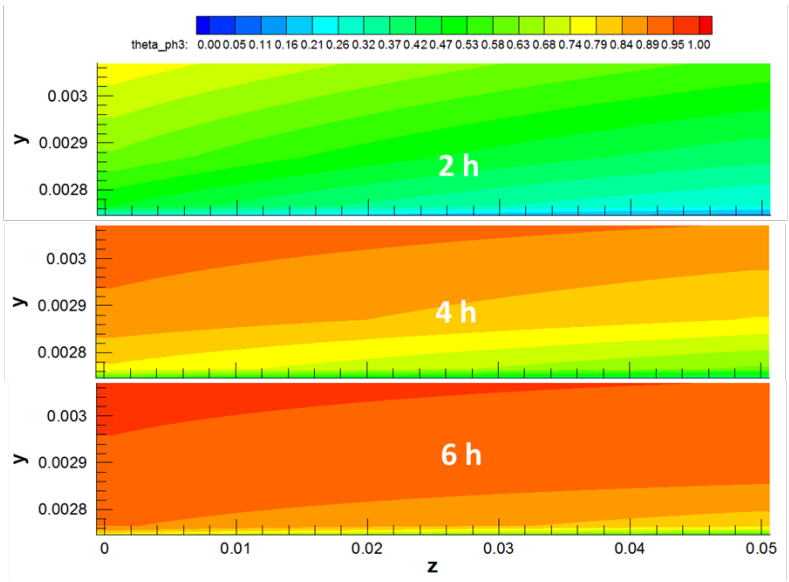

Figure 2. 5: Contours of phosphine coverage at x/2 (y-z plane) after 2 hours (top), 4 hours (middle) and 6 hours (bottom).

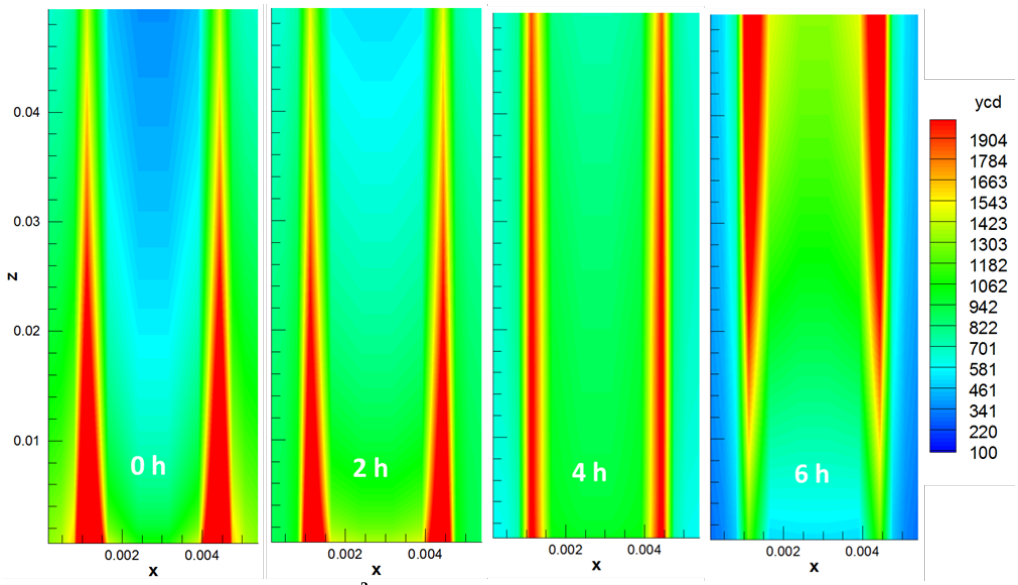

Figure 2. 6: Contours of current density (A/m^2) at anode/electrolyte interface at steady state (top-left) after 2 hours (top-right), 4 hours (bottom-left) and 6 hours (bottom-right) of phosphine exposure

Additional simulations are performed to study the electrochemical behavior of the cell at different times of the gradual performance loss. The V-I behavior and the impedance response of the cell at different stages of gradual anode degradation process are shown in Figure 2.7. The results show that the initial changes in V-I curves with exposure time were mostly due to increase in activation losses. The calculated impedance results (Figure 2.7b) also indicate the polarization resistance first increases then decreases before eventually it starts increasing at a faster rate. This was an unexpected behavior which may be a peculiarity of planar cells. These observations are consistent with the impedance analyses. The current redistribution and the temperature variation are the key physical behaviors that make the planar cell perform better than the button cell. Comparison of Figure 2.7b with Figure 3.3 indicate that the 2nd arc

detected in the experiments in the low frequency range is not captured in the simulations. This might be due to insufficient resolution in the simulations.

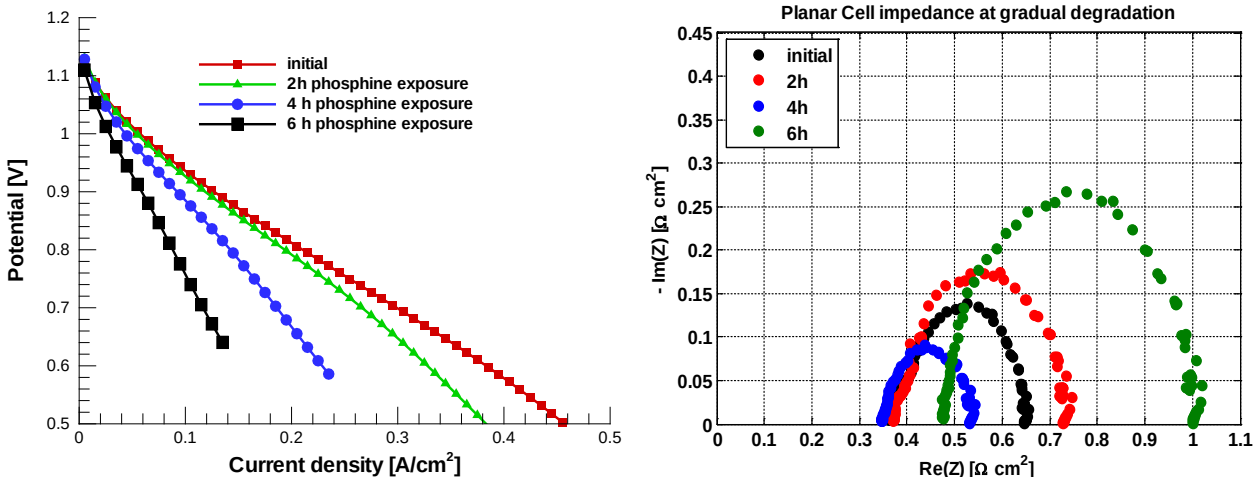

Figure 2.7: Predicted V-I curves of planar cell at different times of phosphine exposure for dry hydrogen(left), predicted impedance curves for planar cell at different time of phosphine exposure (initial, 2h, 4h, 6h): Nyquist representation (right)

Nickel Migration

A transport model for nickel migration is formulated based on mechanisms of electromigration, diffusion and formation of secondary phases. This model is integrated with the one-dimensional code for predicting SOFC anode degradation due to fuel impurities. The model parameters that were previously calibrated are used without further adjustment. The influence of current load and humidity on the elemental redistribution is investigated using the current model.

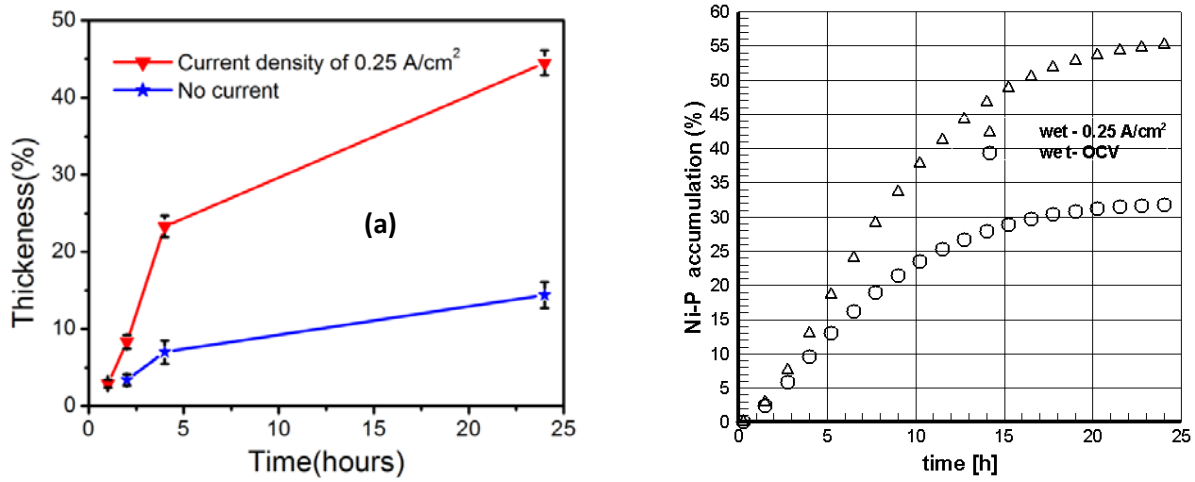

Figure 2. 8: (a) Experiments (Wu et al. 2012): Thickness of the top Ni-P compound layer compared to that of the whole anode layer as a function of time of anode half-cell upon exposure to 5 ppm PH_3 containing coal-syngas at 800 °C. (b) Simulations: the sum of Ni-P (secondary phases) accumulation under (25 % H_2O)at OCV and 0.25 cm^2 current load and dry 0.25 cm^2 current load along gradual degradation time in region I.

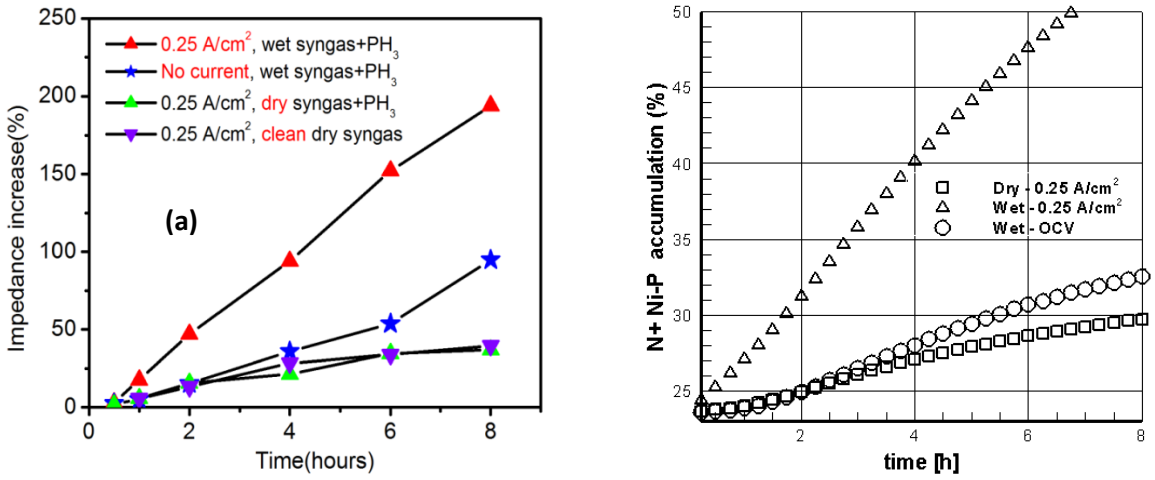

Figure 2. 9: (a) Experiments (Wu et al. 2012): Polarization impedance increases as a function of operation time (5 ppm PH_3 at 800°C): at current density of 0.25A/cm^2, without current load, in dry coal-syngas+PH_3 and in clean dry-coal syngas respectively (b) Simulations: The sum Ni + Ni-P (secondary phases) accumulation under wet (25 % H_2O) at OCV and 0.25 cm^2 current load and dry 0.25 cm^2 current load along gradual degradation time in Region I

In Figure 2.8a, the Ni-P compound layer thicknesses on the anode surface after PH_3 exposure at different current conditions is shown (Experiments by Wu et al.). It can be seen that the Ni-P accumulation is proportional to Ni-P layer thickness. The Ni-P-phase layer thickness and Ni-P accumulation near the surface are observed to increase with the time of anode exposed to PH_3 (Figure 2.8b). The layer thickness and Ni-P accumulation at current density of 0.25 A/cm^2 show faster increase than that without current load. Hence, it can be concluded that the simulated results have a good agreement with the experimental results.

In Figure 2.9a it is seen that, the polarization resistance increases with time at different operation conditions. Polarization resistance is composed of mass transfer losses and activation losses. Mass transfer losses are due to the fuel diffusion limitation at triple phase boundaries. By the formation of secondary phases the diffusion of the fuel decreases during the phosphine exposure. In addition, secondary phases deactivate the available Ni active sites which are related to the activation losses. Furthermore, elemental Ni migration and diffusion from active layer, where electrochemical reaction occurs, accelerate the activation losses. Therefore, the polarization resistance could be proportional to the total Ni migration (Ni elemental transport and Ni-P phases formation). In this context, the results that are obtained from simulation show similar behaviors with the experimental results (Figure 2.9a&b).

A.4. Project 3: Anode Materials Development and Cell-Testing

A.4.1. Objective

The purpose of this work was to evaluate the effect of phosphine on large planar solid oxide fuel cells. Cells were initially tested with pure hydrogen to establish a methodology for cell construction before evaluating a cell with a mixture of hydrogen and 10 ppm phosphine (PH_3). Based on previously published work, the expectation was that the cells would immediately degrade upon introduction of phosphine to the system. The results of these evaluations are presented below.

A.4.2. Testing Setup and Cell Configuration

The fuel cell used was a large, planar cell produced by NexTech Materials, Ltd. It was an electrolyte supported cell with an active area of 32.64 cm^2. For these cells, the anode electrode was 50 µm thick NiO-GDC/NiO-YSZ and the cathode electrode was 50 µm thick LSM/LSM-GDC. The manifolds were machined from a nickel-chromium alloy (Haynes 242) with one gas inlet and one gas exhaust tube of Inconel 601 per manifold. The gases flowed parallel across the cell face rather than directly perpendicular to the cell face. A layer of cobalt was electrodeposited on the surface of each manifold as a protective layer. Mica sheets were cut and used as gaskets to seal the cell. A number of trials were required to determine the optimal number of sheets to seal the cell. Platinum mesh was used as the current collector and attached to the anode and cathode using platinum paint. Platinum wires with silver wire extensions were used as voltage and current taps for the electrical measurements in a four-point configuration. After the cell was assembled, it was placed in a furnace and heated to 800°C at a rate of 1°C/min. During heat-up, nitrogen was fed to the anode and cathode at 100 SCCM. Upon reaching 800°C, the cathode was switched from nitrogen to air at 100 SCCM. The anode was switched to 99 SCCM nitrogen and 1 SCCM hydrogen. Over a four- hour period, the nitrogen flow rate was gradually decreased from 99 to 0 SCCM and the hydrogen flow rate was gradually increased from 1 to 100 SCCM to reduce the anode from NiO to Ni. For testing, air was fed at 300 SCCM to the cathode and hydrogen (or hydrogen/phosphine mixture) at 200 SCCM to the anode.

A.4.3. Testing Results

The trial with phosphine showed lower than expected degradation. At a constant load of 0.1 $A \cdot cm^{-2}$ (the absolute current flow was Figure 3.3a), the average cell degradation rate was constant at 0.026 $mV \cdot h^{-1}$ over the 472 hours of the test (Figure 3.1). The cell maintained OCV near 1.148 V during the entire trial (when the cell was temporarily removed from constant load to complete I-V-P and EIS testing). Phosphine was introduced at Hour 23. At Hour 116, one of the thin-wire voltage taps broke from the cell. This reduced the measurements from 4-point to 2-point measurement. Impedance measurements could no longer be taken and the measuring point for the I-V curves was changed from the cell interfaces to the ends of the manifold inlet and exhaust lines. This added an extra resistance to the line and forced the voltage values to be lowered. Thus, the readings after Hour 116 in Figure 3. 1 were corrected to account for the resistance of the manifold which was assumed to be constant. From the polarization curves (Figure 3.2), the cell's current and power densities decreased slowly over the life of the cell. The drop in power density and current density from Hour 103 to Hour 116 was due to the measuring point change, not the phosphine. The tank containing 10 ppm PH_3 depleted after 472 hours. After the tank was empty, the cell was switched back to pure hydrogen. Measurements were taken after 24 hours (Hour 496) and the cell showed a slight improvement in performance. The last impedance measurement was taken at Hour 93.The impedance spectra (Figure 3.3) at 1.0 A absolute current showed no discernable pattern of resistance increasing or decreasing over time. There are indications of diffusion limitations within the low frequency portion of the plot.

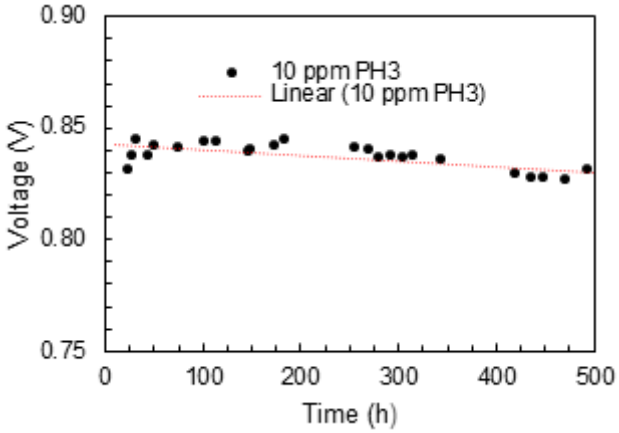

Figure 3. 1: Cell voltage over time at 0.1 A cm^{-2} with 10 ppm phosphine (voltages after Hour 93 are corrected due to one of the cell taps breaking). Degradation rate was 0.026 $mV \cdot h^{-1}$

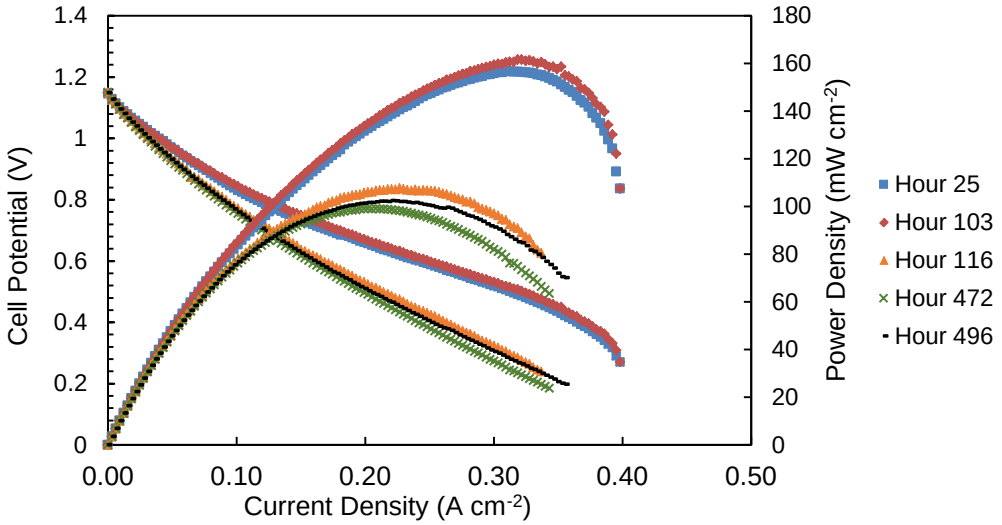

Figure 3.2: Hour 25 was the second hour of phosphine exposure. Hour 116 was the first measurement from the new measuring point on the manifold. Hour 472 was the last measurement with phosphine. Hour 496 was pure hydrogen.

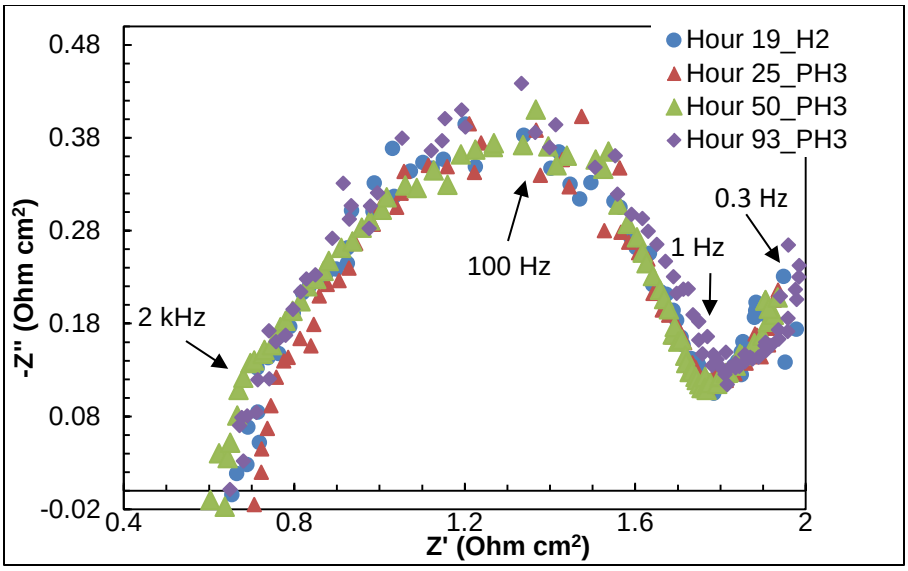

Figure 3.3: Nyquist plot of impedance spectrum before and after exposure to 10 ppm PH_3, until voltage/current taps broke.

A.4.4. Discussion

The observed cell degradation rate of 0.026 $mV \cdot h^{-1}$ was lower than expected; this is in comparison to other data presented in the literature and our team's own modeling predictions. The anode supported cell in Xu et al. (2009) had an anode nearly 1 mm thick and reported a degradation rate of 0.46 $mV \cdot h^{-1}$. The anode thickness in the present experiment was orders of magnitude smaller (at 50 µm). Any phosphine reaching the anode surface should have significantly reduced the cells performance by irreversibly reacting with the Ni in the anode. After 450 hours of phosphine exposure, the cell was switched back to pure hydrogen. The cell showed increased performance after the switch, indicating that there was no permanent damage from the phosphine. Initially, it was speculated that the piping running from the supply tanks to the manifold inlet, the manifold inlet, and/or the manifold itself were absorbing all of the phosphine before it could reach the anode. A Honeywell Toxipro PH_3 single-gas detector was used to measure the exhaust at the anode during the test to check for the presence of phosphine. The sensor indicted a value near 10 ppm (but, measurement error of the sensor still needs to be confirmed). This indirectly confirmed that phosphine was reaching the cell and not being absorbed before contacting the anode or circumventing the anode in any other way.

Previous testing by other researchers has indicated that steam was needed along with the fuel gas in order for the phosphine to have deleterious effects. For the current test, the fuel gas was fed without any steam, i.e. "dry". However, a substantial amount of water was generated from the higher utilization rate of 12.5% for the H_2 fuel. This utilization is much higher than most of the previously-cited tests in literature. The concentration profiles (Figure 3.4) after 2 hours of phosphine exposure, provided by CFD models of Sezer and Celik in this work, showed that directly at the cell inlet, there is still 2 mol% H_2O, which is close to the 3% feed of the other tests. Moreover the water concentration at the outlet end of the cell was nearly 16 mol%. Thus, the average water content equals or exceeds the water present during previous button cell tests (where the initial fuel contains 3% H_2O and the average utilization is ~0.6%, as in the Xu *et al.* work).

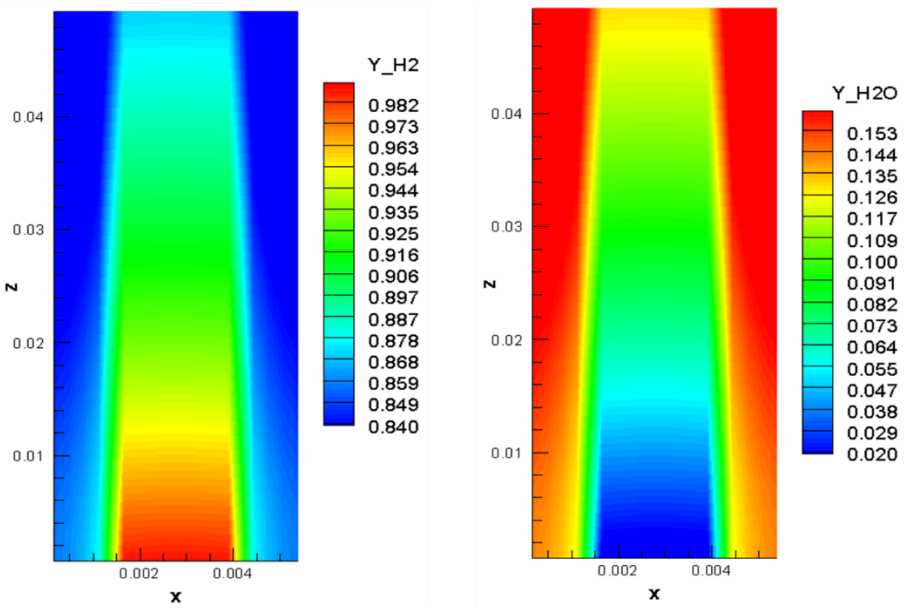

Figure 3.4: Contours of mole fraction at the anode/electrolyte interface (provided by Hayri Sezer)

More work is necessary in order to elucidate the reasons for the unexpected findings mention above. All these experiments should be repeated to better understand if the effect is related to the delivery orientation, load level (and steam content), and interconnect/manifold composition). Additionally, microstructure analysis, chemical analysis, and surface characterization should be performed using SEM, XRD, and XPS to determine phosphine deposition as a function of distance along the cell.

Appendix B

Personnel, Publications, Presentations, Current and Pending Research Projects

Direct Utilization of Coal Syngas in High Temperature Fuel Cells
DOE-EPSCoR-WV State Implementation Program

Richard Bajura (Adm. P.I.), Ismail B. Celik, (P.I.)

Co-PI's:

Nick Wu , Bruce Kang, Harry Finklea , Xueyan Song,

Ed Sabolsky , John Zondlo, Xingbo Liu

SUMMARY:

- **10 Faculty (with 4 newly young faculty recruited for this and related areas of research, all 4 of those faculty have already been promoted to Associate Professor level)**
- **10 Post -doctoral fellows**
- **16 Fully or partially funded graduate students**
- **39 Journal papers published**
- **43 Presentations/Posters/Conference papers**
- **19 Current or pending related research projects**

Projects/Personnel

The research effort is divided into the following three broad projects:

- Project 1. Characterization of the contaminant effects;
- Project 2. Continuum Modeling; and,
- Project 3. Anode Materials Development.

The participants in this research are listed in Table B.1.

Table B.1: List of Investigators and their roles

Investigator	Affiliation*	Project I	Project II	Project III	Comments
PIs					
Richard A. Bajura	NRCCE				Management
I. Celik	BMSCEMR MAE		✓		Management
B. Kang	BMSCEMR MAE	✓	✓		Management
X. Liu	BMSCEMR MAE	✓		✓	
N. Wu	BMSCEMR MAE	✓			New Faculty
E. Sabolsky	BMSCEMR MAE	✓		✓	New Faculty
J. Zondlo	BMSCEMR CHE	✓		✓	
H. Finklea	Chem	✓			
X. Song	BMSCEMR MAE	✓			New Faculty
Andrei Smirnov	BMSCEMR MAE	✓			New Faculty (Now in B&W)
Post Doctoral Fellows					
S. Raju Pakalapati	BMSCEMR MAE		✓		
Chunchuan Xu	BMSCEMR CHE	✓		✓	
Mingyang Gong	BMSCEMR MAE			✓	
Nihan Cayan	BMSCEMR MAE		✓		
Yasemin Vural	BMSCEMR MAE		✓		
Francisco Elizalde Blancas	BMSCEMR MAE		✓		
Mingjia Zhi	BMSCEMR MAE	✓			
Oktay Demircan	Chem	✓			Now at BUniv-Istanbul
Ning Ma	PHYS				Now at NIH
Tao Yang	BMSCEMR MAE		✓		

Graduate Research Students					Status
Francisco Elizalde Blancas	BMSCEMR MAE		✓		Graduated
Nihan Cayan	BMSCEMR MAE		✓		Graduated
Mingyang Gong	BMSCEMR MAE				Graduated
Wenyuan Li	BMSCEMR MAE				
Jinlong Yan	BMSCEMR MAE	✓			Graduated
Philip Gansor	BMSCEMR MAE				Graduated
Hayri Sezer	BMSCEMR MAE		✓		*Current*
Huang Guo	BMSCEMR MAE	✓			Graduated
Wei Zhang	ECAS, Chem	✓			*Current*
Mahfuzur Jony	ECAS, Chem	✓			
Song Chen	BMSCEMR MAE	✓			Graduated
Gulfham Iqbal	BMSCEMR MAE	✓	✓		Graduated
Borja Cantero-Tubilla	BMSCEMR MAE				Left-WVU
Savan Suri	BMSCEMR MAE				
Shimeng Hao	BMSCEMR MAE				
Rolando Chavez	BMSCEMR MAE		✓		Changed subject

Acronyms used: NRCCE (National Research Center for Coal and Energy at WVU); BMSCEMR (Benjamin M. Statler College of Engineering and Mineral Resources); MAE (Department of Mechanical and Aerospace Engineering); CHE (Department of Chemical Engineering); ECAS (Eberly College of Arts and Sciences) ***Chem*** (***Department of Chemistry); PHYS (Department of Physics)***

List of Journal Papers

1- Wenyuan Li, Mingyang Gong, Xingbo Liu: H_2 Oxidation on Doped Yttrium Chromites/ Yttrium Stabilized Zirconia Anode of Solid Oxide Fuel Cell, Journal of Power Sources 241 (2013) 494-501

2- Wenyuan Li, Mingyang Gong, Xingbo Liu: Characterization of doped yttrium chromites as electrode for solid oxide fuel cell by impedance method, Submitted to Journal of Power Sources (2013)

3- Bruce Kang, Huang Guo, Gulfam Iqbal, Ayyakkanna Manivannan, "CO2 Conversion into C/CO using ODF Electrodes with SOEC," Advances in Materials Science for Environmental and Energy Technologies: Ceramic Transactions, Volume 236, 2012.

4- Gulfam Iqbal, Huang Guo, Bruce S. Kang, and Olga A. Marina, "Durability Prediction of Solid Oxide Fuel Cell Anode Material under Thermo-mechanical and Fuel Gas Contaminants Effects," *International Journal of Applied Ceramic Technology*, 8 [1] 13-22, 2011.

5- Huang Guo, Gulfam Iqbal, and Bruce S. Kang, "Effects of PH3 Contaminant on SOFC Performance and Related Anode Surface Temperature Measurements," *International Journal of Applied Ceramic Technology*, 8 [1] 68-73, 2011.

6- Huang Guo, Gulfam Iqbal, and Bruce S. Kang, "Investigation of Secondary Phases due to PH3 Interaction with SOFC Anode," Advances in Materials Science for Environmental and Nuclear Technology II: *Ceramic Transaction*, Volume 227 51-60, 2011.

7- Gulfam Iqbal, Suryanarayana Raju Pakalapati, Francisco Elizalde-Blancas, Huang Guo, Ismail Celik, and Bruce S. Kang, "PEN Structure Thermal Stress Analysis for Planar-SOFC Configurations under Practical Temperature Field," Advances in Materials Science for Environmental and Nuclear Technology II: *Ceramic Transaction*, Volume 227 61-68, 2011.

8- Huang Guo, Gulfam Iqbal, and Bruce S. Kang, "Development of an In-situ Surface Deformation and Temperature Measurement Technique for SOFC Button Cell," *International Journal of Applied Ceramic Technology*, 7 [1] 55-62, 2010.

9- Gulfam Iqbal, and B.S. Kang, "Elastic Brittle Damage Model for Ni-YSZ and Predicted Stress-Strain Relations as a Function of Temperature and Porosity," ASME Journal of Fuel Cell Sciences and Technology, 8(5), Jun 13, 2011.

10- M. Zhi, X. Chen, H. Finklea, I. Celik, N. Qu. Wu, "Electrochemical and Microstructural Analysis of Ni-Yttria Stabilized Zirconia Electrode Operated in Phosphorus-Containing Syngas," *Journal of Power Sources*, 183, 485-490 (2008).

11- S. Chen, Y. Chen, H. Finklea, G. Hackett, X. Song, Kirk Gerdes "Crystal defects of yittria-stabilized zirconia in the solid oxide of fuel cells and their evolution upon cell operation", Solid State Ionics, 206, 104-111 (2012).

12- Y. Chen, S. Chen, H. Finklea, X. Song, G. Hackett, K. Gerdes, "Microstructure and chemistry evolution of triple phase boundaries in the anode of solid oxide fuel cells", Solid State Ionics, 204-205, 87-90, (2011).

13- E. M. Sabolsky, P. Gansor, E. Çiftyürek, K. Sabolsky, C. Xu , and J.W. Zondlo, "In situ Formation of a Solid Oxide Fuel Cell (SOFC) Cermet Anode by $NiWO_4$ Reduction," *Journal of Power Sources* 237, 33-40 (2013).

14- P. Gansor, K. Sabolsky, J. W. Zondlo, and E. M. Sabolsky, "$Sr_2MgMoO_{6-\delta}/Gd_{0.1}Ce_{0.9}O_{1.95}$ composite anode-supported solid oxide fuel cell (SOFC)," Materials Letters 105 (2013) 80–83

15- P. Gansor, C. Xu, K. Sabolsky, J. W. Zondlo, and E. M. Sabolsky, "Phosphine Impurity Tolerance of $Sr_2MgMoO_{6-\delta}$ Composite SOFC Anodes," *Journal of Power Sources* 198, 7-13 (2012).

16- C. Xu, P. Gansor, J.W. Zondlo, K. Sabolsky and E.M. Sabolsky, "An H_2S-Tolerant Ni-GDC Anode with a GDC Barrier Layer for SOFC Applications," *Journal of Electrochemistry Society* 158 [11], B1405-B1416 (2011).

17- C. Xu, J.W. Zondlo, and E.M. Sabolsky, "A Prefilter for Mitigating PH_3 Contamination of a Ni-YSZ Anode," *Journal of Power Sources* 196, 7665-72 (2011).

18- Y. Chen, S. Chen, G. Hackett, H. Finklea, J. Zondlo, I. Celik, X. Song, and K. Gerdes, "Microstructure Degradation of YSZ in Ni/YSZ Anodes of SOFC Operated in Phosphine-containing Fuels," *Solid-State Ionics* 234, 25-32 (2013).

19- C. Xu, J. Zondlo, M. Gong, and X. Liu "Effect of PH_3 Poisoning on a Ni-YSZ Anode-supported Solid Oxide Fuel Cell Under Various Operating Conditions," *Journal of Power Sources* 196, 116-125 (2011).

20- D. Dong, M. Gong, C. Xu, N. Baxter, Y. Li, J. Zondlo, K. Gerdes and X. Liu "Electrochemical Characteristics of Samaria-doped Ceria Infiltrated Strontium-doped $LaMnO_3$ Cathodes with Varied Thickness for Yttria-stabilized Zirconia Electrolytes," *Journal of Power Sources* 196, 2551-2557 (2011).

21- M. Gong, D.Bierschenk, J. Haag, K.R. Poeppelmeirr, S.A. Barnett, C. Xu, J.W. Zondlo and X. Liu, "Degradation of $LaSr_2Fe_2CrO_9$ SOFC Anodes in Phosphine-Containing Fuels," *Journal of Power Sources* 195, 4013-4021 (2010).

22- C. Xu, M. Gong, J.W. Zondlo, X. Liu and H.O. Finklea, "The Effect of HCl in Syngas on Ni-YSZ Anode-Supported Solid Oxide Fuel Cells," *Journal of Power Sources* 195, 2149-2158 (2010).

23- O. Demircan, W. Zhang, C. Xu, J. Zondlo and H.O. Finklea "The Effect of Overpotential on Performance Degradation of the SOFC Ni/YSZ Anode During Exposure to Syngas with Phosphine Contaminant", The Journal of Power Sources, 195, 3091-3096 (2010).

24- C. Xu, J.W. Zondlo, M. Gong, F.E. Blancas, X. Liu, and I.B. Celik, "Tolerance Tests of H_2S-laden Biogas Fuel on Solid Oxide Fuel Cells," *Journal of Power Sources* 195, 4583-4592 (2010).

25- C. Xu, J.W. Zondlo, H.O. Finklea, O. Demircan, M.Gong and X. Liu, "The Effect of Phosphine in Syngas on Ni-YSZ Anode-Supported Solid Oxide Fuel Cells,"*Journal of Power Sources* 193, 739-746 (2009).

26- O. Demircan, C. Xu, J. Zondlo, and H.O. Finklea "In-situ Van der Pauw Measurements of the Ni/YSZ Anode During Exposure to Syngas with Phosphine Contaminant," *Journal of Power Sources* 194, 214-219 (2009).

27- Cayan F.N., Zhi M., Pakalapati S.R., Celik I., Wu N., Gemmen R., Effects of Coal Syngas Impurities of Solid Oxide Fuel Cells, *Journal of Power Sources*, 185, 595-602 (2008).

28- Cayan F.N., Pakalapati S.R., Elizalde-Blancas F., Celik I., On Modeling Multi-Component Diffusion Inside the Porous Anode of Solid Oxide Fuel Cells Using Fick's Model, *Journal of Power Sources*, 192, 467-474 (2009).

29- Cayan, F., Pakalapati, S. R., Celik, I., Xu, C., and Zondlo, J., A Degradation Model For Solid Oxide Fuel Cell Anodes Due To Impurities In Coal Syngas: Part I Theory And Validation, *Fuel Cells*, v 12, n 3, p 464-473 (2012).

30- J. Yan, X. Chen, S. Suri, M. Zhi, Effects of Electric Current and Moisture on Degradation of Nickel/Yttria-Stabilized Zirconia Fuel-Cell Anode in Phosphine-Containing Coal Syngas, submitted to J. Power Sources.

31- Electrochemical Behavior of Patterned Nickel Micro-strip Anode in Phosphine-Containing Coal Syngas, to be prepared.

32- C. Xu, J. W. Zondlo, H. O. Finklea, O. Demircan, M. Gong, X. Liu, "Poisoning mechanism of Ni-YSZ anode-supported solid oxide fuel cell by PH_3 impurity in syngas fuel," *Preprints of Symposia - American Chemical Society, Division of Fuel Chemistry*, Volume 54, Issue 2, Pages 814-815 (2009)

33- J. A. Escobar, S. R. Pakalapati, I. B. Celik, H. Finklea, "A correction for impedance measurements using the three point electrode technique in SOFCs," *ECS Transactions*, Volume 25, Issue 2, Solid Oxide Fuel Cells 11 (SOFC-XI), Pages 391-400 (2009).

34- O. A. Marina, L. R. Pederson, R. Gemmen, K. Gerdes, H. Finklea, I. B. Celik, "Overview of SOFC anode interactions with coal gas impurities," *ECS Transactions*, 26, 363-370 (2010).

35- M. Zhi, F. N. Cayan, I. Celik, R. Gemmen, S. R. Pakalapati, N. Q. Wu, Temperature and impurity concentration effects on degradation of nickel/yttria-stabilized zirconia anode in PH3-containing coal syngas, *Fuel Cells*, 10 (2010), 174-180

36- From a Single Cell to a Stack Modeling, Fuel Cells and Hydrogen Energy: Modeling Solid Oxide Fuel Cells, by I.B.Celik and S.R.Pakalapati , R.Bove and S.Ubertini (eds),Springer Science and Business Media B.V.2008, pp.123-182.

37- Yun Chen, Song Chen, Gregory Hackett, Harry Finklea, John Zondlo, Ismail Celik, Xueyan Song, Kirk Gerdes, "Microstructure origin of electrochemical degradation of SOFC anodes operated in phosphine-containing fuels," *Solid State Ionics*, 234, 25-32 (2013).

38- Suryanarayana Pakalapati[a,b], Kirk Gerdes[a], Harry Finklea[a,c], Mingyang Gong[a,b], Xingbo Liu[a,b], Ismail Celik[a,b] ,"Micro scale dynamic modeling of LSM/YSZ composite cathodes", *Solid State Ionics*, 258, 45-60 (2014).

39- Sezer, H., Celik, I, B., " Phosphine induced Nickel Migration in SOFC Anodes: A Computational Study", (manuscript is being reviewed by the Journal of Electrochemical Acta)

List of Conference Papers/Posters/Presentataions

1- Pakalapati, S.R., Yavuz, I., Elizalde-Blancas, F., and Celik, I. (2006) "Comparison of a Multi-Dimensional Model with a Reduced Order Pseudo Three-Dimensional Model for Simulation of Solid Oxide Fuel Cells", Proceedings of the 4th International ASME Conference on Fuel Cell Science, Engineering and Technology, Irvine, California, June 19-21.

2- Elizalde-Blancas, F., Yavuz, I., Pakalapati, S.R., Celik, I., (2006) "Effect of Channel Height on the Performance of a Solid Oxide Fuel Cell", Proceedings of the 4th International ASME Conference on Fuel Cell Science, Engineering and Technology, Irvine, California, June 19-21.

3- S. R. Pakalapati, F. Elizalde-Blancas, I. Celik, "Numerical Simulation of Solid Oxide Fuel Cell Stacks: Comparison between a Reduced Order Pseudo Three-dimensional Model and a Multidimensional Model", Proceedings of the 5th International Conference on Fuel Cell Science, Engineering, and Technology, June 18-20, 2007, Brooklyn, NY.

4- F. Elizalde-Blancas, S. R. Pakalapati, F. N. Cayan, I. B. Celik, "One-Dimensional Transient Lumped Model for Fast Fuel Cell Stack Analysis", Proceedings of the Renewable Energy Symposium and Expo, September 14-15, 2007, Frostburg, MD.

5- M. Zhi, N. Madhiri, H. Finklea, I. Celik, B. Kang, X. Liu, C. Johnson, N. Wu, "Effects of Phosphorous Impurity on Performance of Ni-YSZ Anode of SOFC", Proceedings of the 212th Electrochemistry Society Meeting, Washington. D.C.,October 7-12,2007.

6- M. Zhi*, H. Finklea, N. Madhiri, I. Celik, B. Kang, X. Liu, N. Q. Wu, Impedance analysis of phosphorous impurity effects on performance of Ni-YSZ anode of SOFC, 212th ECS Meeting, Washington, DC, October 7-12, 2007, (oral presentation).

7- F.N.Cayan, M.Zhi, S.R.Pakalapati, I.Celik and N.Wu, "Effects of Coal Syngas Contaminants on SOFC Anodes: A Review", Proceedings of Symposium on Coal Based Fuel Cell Technology: Status, Needs and Future Applications", Morgantown, October 11-12, 2007.

8- S. R. Pakalapati, F. Elizalde-Blancas, I. B. Celik, "Modeling of a Coal Syngas Based SOFC", Proceedings of Symposium on COAL BASED FUEL CELL TECHNOLOGY: Status, Needs and Future Applications, October 11-12, 2007, Morgantown, WV.

9- Cayan F.N., Pakalapati S.R., Celik I., Modeling of Diffusion Inside the Porous Electrodes, Proceedings of the Second European Fuel Cell Technology and Applications Conference EFC2007, Rome, December 11-14, 2007.

10- M. Zhi*, N. Q. Wu, Degradation of Ni-YSZ anode in phosphorous-containing coal syngas, Army Research Office Workshop on soldier-portable power sources, College Park, MD, Feb.20-21, 2008, (poster).

11- Cayan F.N., Pakalapati S.R., Elizalde-Blancas F., Celik I., On Modeling Multi-Component Diffusion Inside the Porous Anode of Solid Oxide Fuel Cells Using Fick's Model, Proceedings of

the 6th International Fuel Cell Science, Engineering and Technology Conference, Denver, CO June 16-18, 2008.

12- Elizalde-Blancas F., Pakalapati S. R., Escobar-Vargas J., Celik I. B., Numerical Evaluation and Comparison of Different Reduced Mechanisms for Predicting the Performance of a SOFC Operating on Coal Syngas, Proceedings of the ASME Fluids Engineering Division Summer Conference, Jacksonville, Florida, August 10-14, 2008.

13- F.N. Cayan, M.Zhi., , S.R Pakalapati, I.Celik, , N.Wu and R.Gemmen, (2008), Effects of Coal Syngas Impurities of Solid Oxide Fuel Cells: A Review, Proceedings of International Pittsburgh Coal Conference, September 29-October 2, 2008, Pittsburgh, PA.

14- F.N. Cayan, S.R. Pakalapati, F. Elizalde-Blancas, I.B. Celik, A Phenomenological Model for Degradation of Solid Oxide Fuel Cell Anodes due to Impurities in Coal Syngas, Proceedings of the Seventh International Fuel Cell Science, Engineering and Technology Conference, Newport Beach, CA, USA, June 8-10, 2009.

15- J. A. Escobar, S. R. Pakalapati, J. R. Nanduri, I. B. Celik, Direct Simulation of Mass Transport in a SOFC Cathode using Microchannels, Proceedings of the Seventh International ASME Conference on Nanochannels, Microchannels and Minichannel (ICNMM2009), Pohang, South Korea, June 22-24, 2009.

16- I. Celik, F. Elizalde-Blancas, S. Pakalapati, F. Cayan, Numerical Prediction of SOFCs Performance Operating on Coal Syngas, Proceedings of the European Fuel Cell Forum, Lucerne, Switzerland, June 29 – July 2, 2009.

17- F. Elizalde-Blancas, S.R. Pakalapati, F.N. Cayan, I. B. Celik, Numerical Simulations of Solid Oxide Fuel Cells Operating on Coal Syngas: A Parametric Study, Proceedings of the 2009 ASME Fluids Engineering Division Summer Meeting, Vail, CO, August 2-6, 2009.

18- F. N. Cayan, M. Zhi, S. R. Pakalapati, N. Wu and I. B. Celik, Secondary Phases of P-Impurity in SOFC Anode Operating on Coal Syngas, Poster presented at the 26th Annual International Pittsburgh Coal Conference, Pittsburgh, PA, September 20-23, 2009 (paper published in the proceedings).

19- J. A. Escobar, S. R. Pakalapati, I. B. Celik, H. Finklea, “A Correction for Impedance Measurements using the Three Point Electrode Technique in SOFCs”, 216th Electrochemical Society Meeting, SOFC XI, Vienna, Austria, October 4-9, 2009.

20- O.A. Marina, L.R. Pederson, R. Gemmen, K. Gerdes, H. Finklea, I. Celik, Overview of SOFC Anode Interactions with Coal Gas Impurities, Presented at 2009 Fuel Cell Seminar and Exposition, Palm Springs, CA, November 16-19.

21- M. Zhi, N.Q. Wu, Degradation Mechanism of Nickel-Yttria Stabilized Zirconia SOFC Anode Materials in PH3 Containing Coal Syngas, 218th ECS Meeting, Las Vegas, NV, Oct.10-15, 2010, (oral presentation).

22- S. Pakalapati, I. Celik, H. Finklea, M. Gong, and X. Liu (2011) “A Micro-Scale Model for Oxygen Reduction on LSM-YSZ Cathode”, ECS Transactions, 35(1):963-976.

23- Iqbal, G., Pakalapati, S. R., Elizalde-Blancas, F., Guo, H., Celik, I. B., Kang, B., "PEN structure

thermal stress analysis for planar-SOFC configurations under practical temperature field," Ceramic Transactions, v 227, p 61-68, 2011, Advances in Materials Science for Environmental and Nuclear Technology II.

24- Cayan, F. N., Pakalapati S. R., and Celik, I. B., "Modeling Degradation of Solid Oxide Fuel Cell Anodes due to Impurities in Coal Syngas," ASME 9th Fuel Cell Science Engineering and Technology Conference, Washington DC, Aug 7-10, 2011.

25- Fatma N. Cayan, Suryanarayana R. Pakalapati and Ismail Celik (2011) "A Degradation Model for Solid Oxide Fuel Cell Anodes due to Impurities in Coal Syngas", 9th Fuel Cell Science, Engineering and Technology Conference, August 7-10,Washington,DC.

26- Francisco Elizalde Blancas, Suryanarayana R. Pakalapati, Fatma N. Cayan, Ismail B. Celik, *Numerical Modeling of an Anode Supported Button SOFC,* XVII Congreso Internacional de la SOMIM, San Luis Potosí, San Luis Potosí, Mexico, September 21-23, 2011.

27- Francisco Elizalde-Blancas, Ismail B. Celik, Victor H. Rangel-Hernandez, Abel Hernandez-Guerrero, *Numerical Modeling of SOFCs Operating on Biogas from Biodigesters,* European Fuel Cell – Piero Lunghi Conference & Exhibition, December 14-16, 2011, Rome, Italy.

28- Suryanarayana R. Pakalapati, Yasemin Vural, Chunchuan Xu, John Zondlo, Ismail Celik, "Three-Dimensional Modeling of a SOFC Operating on Biogas", ASME 9th International Fuel Cell Science Technology and Engineering Conference, Washington D. C., August 7-10, 2011.

29- Suryanarayana R. Pakalapati, Ismail B. Celik, Harry O. Finklea, Jose A. Escobar-Vargas, "A Computational Study of Anomalous Cathode-Reference Voltages on Anode Supported Button SOFCs," ECS Transactions, proceedings of 221st ECS Meeting, Seattle, Washington, May 6 - May 10, 2012.

30- Harry Finklea, Xiaoke Chen, Ismail Celik, Suryanarayana Pakalapati, Kirk Gerdes, and Yun Chen "1D and 2D simulation of impedances in an anode-supported SOFC", 221st ECS Meeting, Seattle, Washington, May 6 - May 10, 2012.

31- Yasemin Vural, Suryanarayana Pakalapati, Ismail Celik, "A Continuity Outlet Boundary Conditiion for the Lattice Boltzmann Method," Proceedings of the ASME 2012 Fluids Engineering Division Summer Meeting, July 8 – 12, 2012, Rio Grande, Peurto Rico.

32- Suryanarayana Pakalapati , Kirk Gerdes, Harry Finklea, Mingyang Gong, Xingbo Liu, Ismail Celik, "Micro Scale Dynamic Modeling of LSM/YSZ Composite Cathodes," 13th Annual Solid State Energy Conversion Alliance (SECA) Workshop, July 24-27, 2012, Pittsburgh, PA.

33- R. Bajura, I. Celik, H. Finklea, B. Kang, X. Liu, E. Sabolsky, X. Song, N. Wu, J. Zondlo, M. Song, S. Pakalapati, C. Xu, M. Zhi, "Recent Progress in Coal Syngas Contaminant Effect Studies on SOFC Anodes at West Virginia University," 13th Annual Solid State Energy Conversion Alliance (SECA) Workshop, July 24-25, 2012, Pittsburgh, PA.

34- Sezer, H., Pakalapati, S.R., Guo, H., Kang, B., Celik, I. B., "A Computational Study on the effect of the Steam on SOFC Anode Degradation Due to Phosphine," 13th Annual Solid State Energy Conversion Alliance (SECA) Workshop, July 24-25, 2012, Pittsburgh, PA.

35- M. Zhi and N. Q. Wu, One-dimensional nanostructures for solid oxide fuel cell, 2012 MRS Fall Meeting, Boston, MA, November 25-30, 2012, (oral presentation).

36- H. Finklea, M. Zhi, High Temperature Environmental Scanning Electron Microscopy of Ni/YSZ surfaces after exposure to PH3, 2013 Fall MRS meeting, Boston, MA, Dec.1-6, 2013

37- Sezer, H., Pakalapati, S. R., Celik, I., "The effect of steam concentration on phosphine induced sofc anode degradation: a computational study," in *5th International Conference on Fundamentals & Development of Fuel Cells* , Karlsruhe, 2013

38- Sezer, H., Pakalapati, S. R., Celik, I., " Phosphine induced anode performance degradation in planar SOFC: A numerical study", in 13th International Symposium on Solid Oxide Fuel Cells (SOFC-XIII), Okinawa, Japan, 2013

39- H. Sezer, I. B. Celik, S. R. Pakalapati, "Sensitivity Analysis of a one-Dimensional SOFC Contaminant Degradation Model Using Dual Numbers Automatic Differentiation", 225th ECS Meeting, Orlando, Florida, 2014.

40- H. Sezer, T. Yang, I. B. Celik, "Electrochemical Evaluation of a Planer SOFC under Phosphine Induced Degradation", 15th Annual Solid State Energy Conversion Alliance (SECA) Workshop, July 22-23, 2014, Pittsburgh, Pennsylvania (Poster presentation)

41- H. Sezer, I. B. Celik, T. Yang, S. R. Pakalapati, "Analysis of Polarization and Impedance Under Phosphine Induced Anode Degradation in a Planer SOFC", 225th ECS Meeting, Orlando, Florida, 2014.

42- Celik, I. B., Sezer, H., Pakalapati, S.R., "Richardson extrapolation using DNAD", American Physical Society 66th annual DFD meeting, Pittsburgh, PA, 2013.

43- Sezer H, Celik, I. B., "A computational study of nickel migration in SOFCs anode due to phosphine induced degradation and applied electrical current", 226th ECS Meeting, Cancun, Mexico, October 5-9, 2014.

Patents

1. **Patent disclosure**: "Pre-Filter for Removal of Trace Contaminants from Gaseous Fuels for Use in Solid Oxide Fuel Cells", C. Xu, J.W. Zondlo, and E.M. Sabolsky, US Patent & Trademark Office, August 2010. Pending.

Honors and Awards

1. Dr. Xingbo Liu and his co-workers won the prestigious R&D 100 award for year 201l for their work on "Electroplated coating for solid oxide fuel cell interconnects"

2. A poster titled "Sulfur tolerant anode for solid oxide fuel cell using coal syngas" by Sean Belardo, an undergraduate reasercher in Dr. Xingbo Liu's team was selected for presentation at 2012

'Posters on the Hill' event conducted by Council on Undergraduate Research at Capitol Hill, Washington D.C., on April 24, 2012.

Current Related Research Projects

1- Cathode Cation Segregation, $96k, 1 year, URS Corporation.(Harry Finklea, PI)

2- "Surface-Plasmon Enhanced Photocatalytic Activity of Metal/Semiconductor Composites for Solar Fuel Production", $388,561, NSF (CBET-1233795), 08/15/2012-07/10/2015

3- EIS Analysis of SOFCs, $36k, 1 year, URS Corporation. (Dr. Finklea, PI)

4- Modeling and Characterization of ORR in SOFC Cathode, funded by URS (Xingbo Liu, PI), no overlap

5- Fundamental Understanding of Oxygen Reduction and Reaction Behavior and Developing High Performance and Stable Heterostructured Cathodes, funded by NETL-SECA program, (Xingbo Liu, PI) no overlap

6- Electrodeposited Mn-Co Alloy Coating for Solid Oxide Fuel Cell Interconnects, funded by DoE-SBIR, (Xingbo Liu, PI) no overlap

7- Development of Self-Powered Wireless-Ready High Temperature Electrochemical Sensors of In-situ Corrosion Monitoring for Boiler Tubes in Next Generation Coal-based Power Generation Systems, funded by NETL-Coal Utilization Science Program, (Xingbo Liu, PI)

8- Department of Energy - NETL, Microstructure Analysis of Cathode, Anode and Electrolyte of SOFC (Song PI)

9- Department of Energy, Novel Nanostructure Tailored Highly Active and Stable Electro-Catalytic Architecture on Surface of Cathode of SOFCs, (Song PI), no overlap

10- Comprehensive Modeling and Improvement in Cathode Performance (X. Liu, PI, E. Sabolsky, Co-PI) - URS Corporation, *$79,870* (01/15/2010 – 12/31/2010) – Completed

11- Microstructural Engineering of Porous SOFC Cathodes (E. Sabolsky, PI)- URS Corporation, *$86,173* (01/01/2011 – 11/14/2011). – Completed

12- Scale-up of Engineered Foam Cathode to SECA Scale (E. Sabolsky, PI)- DOE-NETL (URS Corporation),*$57,132* (03/15/2012 – 02/28/2013)-Completed

13- Scale-up of Engineered Foam Cathode to SECA Scale (E. Sabolsky, PI) - DOE-NETL (URS Corporation), *$36,174* (05/31/2013 – 09/31/2013) – Completed

14- Materials and Methods for Anode Infiltration (E. Sabolsky, PI) - DOE-NETL (URS Corporation), *$66,177* (10/13/2013 – 11/15/2014) – Current

15- Dynamic 3D multi-physics cathode/anode model , URS/NETL, ~$450K(Ismail Celik, PI) current

16- WV Center for Electrochemical Energy Storage: a 5 year project with over $1.5 million funding (P.I. X. Liu and others including Ismail Celik, Co- PI); Celik's Task: Modeling and simulation of fundamental processes within NASICON Batteries,

17- Scalable and Cost Effective Barrier Layer Coating to Improve Performance and Stability of SOFC Cathode, DoE-NETL, $800K (Xingbo Liu, PI), 10/1/2014-9/30/2017

18- Development of an Intermediate Temperature SOFC for Power and Fuel Cogeneration, ARPA-E – Rebels program, $2.8M (Greg Tao-MSRI, PI; Xingbo Liu-WVU, Co-PI), 10/1/2014-9/30/2017

19- Solid Composite Electrolyte to Improve Safety of Li-Ion Batteries for Grid Energy Storage, DoE-OE/PNNL, $100K (Xingbo Liu, PI) 6/1/2014-5/31/2015